DRAFT – DRAFT – DRAFT – DRAFT – DRAFT – DRAFT – DRAFT – DRAFT

Version Date 8/14/01

EXO

an advanced Enriched Xenon double-beta decay Observatory

Letter of Intent

SLAC EPAC

September 2001

M. Breidenbach[8], E. Conti[7], M. Danilov[4], R. DeVoe[3], Z. Djurcic[1], A. Dolgolenko[4], G. Gratta[9](spokesman), T. Koffas[9], M. Moe[5], A. Odian[8], P. Picchi[10], A. Piepke[1], F. Pietropaolo[7], C. Prescott[8], P. Rowson[8], P. Vogel[2], J-L. Vuilleumier[6], S. Waldman[9], Y-F. Wang[9], J. Wodin[9], O. Zeldovich[4]

[1] *Physics Department, University of Alabama, Tuscaloosa AL*
[2] *Bridge Laboratory, Caltech, Pasadena CA*
[3] *Almaden Research Center, IBM, San Jose CA*
[4] *ITEP, Moscow, Russia*
[5] *Physics Dept., UC Irvine, Irvine CA*
[6] *Institut de Physique, Universite de Neuchatel, Switzerland*
[7] *INFN, Sezione di Padova, Padova, Italy*
[8] *Stanford Linear Accelerator Center, Stanford CA*
[9] *Physics Department, Stanford University, Stanford CA*
[10] *Dipartimento di Fisica, Università di Torino, Italy*

Contents

1 Executive Summary **5**

2 Physics Considerations **6**
2.1 Survey of neutrino physics 6
2.2 Cosmological implications 10
2.3 Double-beta decay 10
2.4 Present status of $0\nu\beta\beta$ decay searches 14

3 Detector design concepts **17**
3.1 A high pressure Xe gas TPC Concept 20
3.2 A liquid TPC Concept 23
3.3 Barium spectroscopy and atom tagging 23
3.3.1 Laser Detection of Single Atoms in Atomic Physics 25
3.3.2 Barium Detection in High Pressure Xenon 25
3.3.3 Laser Detection System 28
3.4 Expected backgrounds and Detector Performance 29

4 Detector R&D Program **32**
4.1 Ba^+ optical spectroscopy 32
4.2 Xe purification techniques 34
4.3 Ultimate energy resolution in LXe 36
4.4 Ba^+ extraction 38
4.5 Radioactivity Control 40
4.6 Initial analysis of a ^{136}Xe sample. 40

5 100 kg Prototype Detector **42**

1 Executive Summary

This Letter-of-Intent describes an R&D program to develop a qualitatively new approach to the absolute measurement of neutrino masses through what could be considered as the ultimate double-beta decay experiment. The proponents anticipate that the current R&D activities will lead to a proposal to build and operate a detector to investigate double beta decay in ^{136}Xe with Majorana neutrino mass sensitivity in the 10 meV region.

Recent results from a number of independent experiments [1, 2, 3] can be interpreted as due to finite neutrino masses and, in particular, high statistics measurements of atmospheric neutrinos by the Super-Kamiokande[4] experiment are regarded by most as firm evidence that neutrinos have non-zero masses. In addition, the very recent results from SNO[5], together with Super-Kamiokande solar neutrino data, also suggest finite neutrino masses.

While these measurements, based on oscillations, have set the stage for a systematic study of the intrinsic neutrino properties, only rather crude limits exist on the absolute magnitude of neutrino masses. Indeed, theoretical models span a large range of scenarios, from the degenerate case where mass differences among flavors are small with respect to the absolute mass scale [6], to the hierarchical, where mass differences are of the same order as the mass themselves. However, while the neutrino mass scale is unknown, the present data on oscillations lead rather naturally to masses in the range $0.01 < m_\nu < 1$ eV, as shown recently, e.g. in [7]. In particular, the atmospheric neutrinos which provide the most convincing evidence for neutrino oscillation to date, allow one to establish model independent *lower* limit of ~ 55 meV for the mass of at least one massive neutrino, thus defining the relevant mass scale. In general the measurement of the absolute value of neutrino masses should clearly be considered as one of the most important frontiers of modern particle physics.

It is unlikely that direct neutrino mass measurements, most notably with tritium [8], will be able to reach sensitivities substantially below 1 eV in the near future. In contrast, we will show that a large double-β decay experiment using isotopically enriched ^{136}Xe can reach a sensitivity corresponding to neutrino masses as low as $\sim$0.01 eV. A xenon detector offers the unique possibility of complementing the traditional energy and position measurements with the positive identification the final state, a barium ion, thus providing an essentially background-free measurement of unprecedented sensitivity for the Majorana neutrino mass. The only isotope that can be used in this fashion, ^{136}Xe , is a noble gas at standard conditions and would transmute through double-beta decay into ^{136}Ba. The technique for optically tagging single barium ions has been extensively developed, for different purposes, in the last several years and could be adapted to confirming the occurrence of double-beta decay in a very large TPC system.

While the logistical problems connected with the procurement of a large amount ($\sim$ 10 tons) of isotopically enriched ^{136}Xe are being dealt with under the Nuclear-Non-

Proliferation programs of DoE, here we will concentrate on the detector R&D program required in order to optimize the most effective detector design for the purpose.

2 Physics Considerations

2.1 Survey of neutrino physics

The main issue in neutrino physics today is the question whether neutrinos, like the charged fermions, have a mass. When the Standard Model was established, there was no experimental reason to introduce a neutrino mass, and hence the model postulated that neutrinos are massless. This assumption was consistent with the empirical observation that the individual lepton flavors seem to be conserved (and, naturally, the total lepton number as well). In addition, since the upper limits on neutrino masses are so much smaller than the masses of the corresponding charged leptons (or quarks) it was "natural" to assume that, in fact, neutrinos are massless, hence avoiding the unnaturally small mass ratios. However, at present there is a consensus that the Standard Model cannot be applicable at arbitrarily high energies. Various reasonable extensions of the Standard Model typically predict the existence of neutrino mass. While mass values are not accurately predicted, it appears that neutrino masses in the 0.01 - 1 eV range are preferred, in agreement with the experimental hints described below. Most of such extensions, moreover, lead to the expectation that the massive neutrinos are Majorana particles, and that the phenomenon of mixing, analogous to the Cabibbo-Kobayashi-Maskawa mixing among quarks, will govern their weak interactions.

Conceptually, the simplest way to search for the neutrino mass is based on the kinematic studies of the particles produced in weak decays such as ^{3}H $\rightarrow ^3$He $e^- \bar{\nu}_e$, $\pi \rightarrow \mu\nu_\mu$ and $\tau \rightarrow n\pi\nu_\tau$. The latter two processes result in limits for the mass of ν_μ and ν_τ of, respectively, 170 keV and 18.2 MeV. The limit on the $\bar{\nu}_e$ mass from the tritium beta decay, however, is in the few eV range. While some of the systematic uncertainties leading to best fits in the unphysical range $m_\nu^2 < 0$ seem to have been understood and the design of a next generation spectrometer is being pursued [9], the expected ν_e sensitivity, even in the absence of possible new systematic effects, will be no better than 1/3 eV.

Another conceptually simple neutrino mass determination is based on the time-of-flight method with the supernova neutrinos. Large underground detectors like KamLAND, LVD and Super-Kamiokande[10] will be particularly well equipped to perform such a measurement that, however, requires a supernova explosion in the right region of the universe.

The experimental hints for neutrino mass are at present based on the phenomenon of neutrino oscillations. If, as suggested above, neutrinos are massive particles which behave in analogy to quarks, the states with a definite mass (i.e., the "mass eigenstates" which propagate as plane waves in a vacuum) are not necessarily the partners

of the charged leptons that couple to the vector bosons $W^{\pm}$ in doublets (i.e., the weak eigenstates)

$$\left(\begin{array}{c} \nu_{\rm e} \\ {\rm e}^- \end{array} \right) , \left(\begin{array}{c} \nu_{\mu} \\ \mu^- \end{array} \right) , \left(\begin{array}{c} \nu_{\tau} \\ \tau^- \end{array} \right) . \tag{1}$$

The weak eigenstates $|\nu_l\rangle$ will be in such a case linear superpositions of the mass eigenstates $|\nu_i\rangle$

$$|\nu_l\rangle = \sum_i U_{l,i} |\nu_i\rangle \ , \tag{2}$$

where the coefficients $U_{l,i}$ form the leptonic mixing matrix. If we assume that only three neutrinos can contribute in the Eq. (2) above, then U is a unitary 3×3 matrix.

If Eq. (2) is valid, we encounter the phenomenon of neutrino oscillations in which a neutrino which was initially in the weak eigenstate l can be spontaneously transformed, at least in part, into another weak eigenstate neutrino of flavor l'.

For a simplified two neutrino flavors mix, e.g. e and μ, one finds that the mixing matrix U depends only on one mixing angle θ, and the oscillation probability is given by

$$U = \left(\begin{array}{cc} \cos\theta & \sin\theta \\ -\sin\theta & \cos\theta \end{array} \right) \tag{3}$$

$$P(\nu_{\rm e} \to \nu_{\mu}, L) = \sin^2 2\theta \, \sin^2(\Delta m^2 L/4E) \ . \tag{4}$$

Here $\Delta m^2 \equiv m_1^2 - m_2^2$ and L, E and $m_{1,2}$ are, respectively, the distance traveled by the neutrinos, their energy and the masses of their mass eigenstates.

While most oscillation searches resulted in null results at present, there are three groups of measurements that suggest the existence of neutrino oscillations.

The first group of measurements which are interpreted as evidence for neutrino oscillations deals with the "missing" solar neutrinos. The Sun produces an intense flux of electron neutrinos as a byproduct of the fusion reactions which generate solar power. It is believed that the solar structure is understood sufficiently well so that the flux and energy spectrum of the solar neutrinos can be confidently predicted. The solar neutrino fluxes have been measured in six experiments so far [3, 5]. All of them report a deficit, i.e., the measured flux is less than the expected one. Moreover, the reduction depends on the neutrino energy, inferred experimentally from the thresholds of the individual detectors. In addition the most recent SNO measurement and SuperKamiokande data are sensitive to different linear combinations of ν_e and $\nu_{\mu,\tau}$, so that the combined results of the two experiments can be expressed as measurements of the *total* non-sterile neutrino and ν_e fluxes. The present conclusion is that the total neutrino flux, i.e., the combination of the ν_e flux deduced from SNO (pure charged current) and the excess flux deduced from Super-Kamiokande (assuming that it is due to the neutral current interaction), is in agreement with Standard Solar Model calculations, hence the deficit in the ν_e channel could be explained by neutrino oscillation. While the present SNO data have a significance slightly above 3σ, the oscillation hypothesis offers a very elegant mechanism to interpret all the present

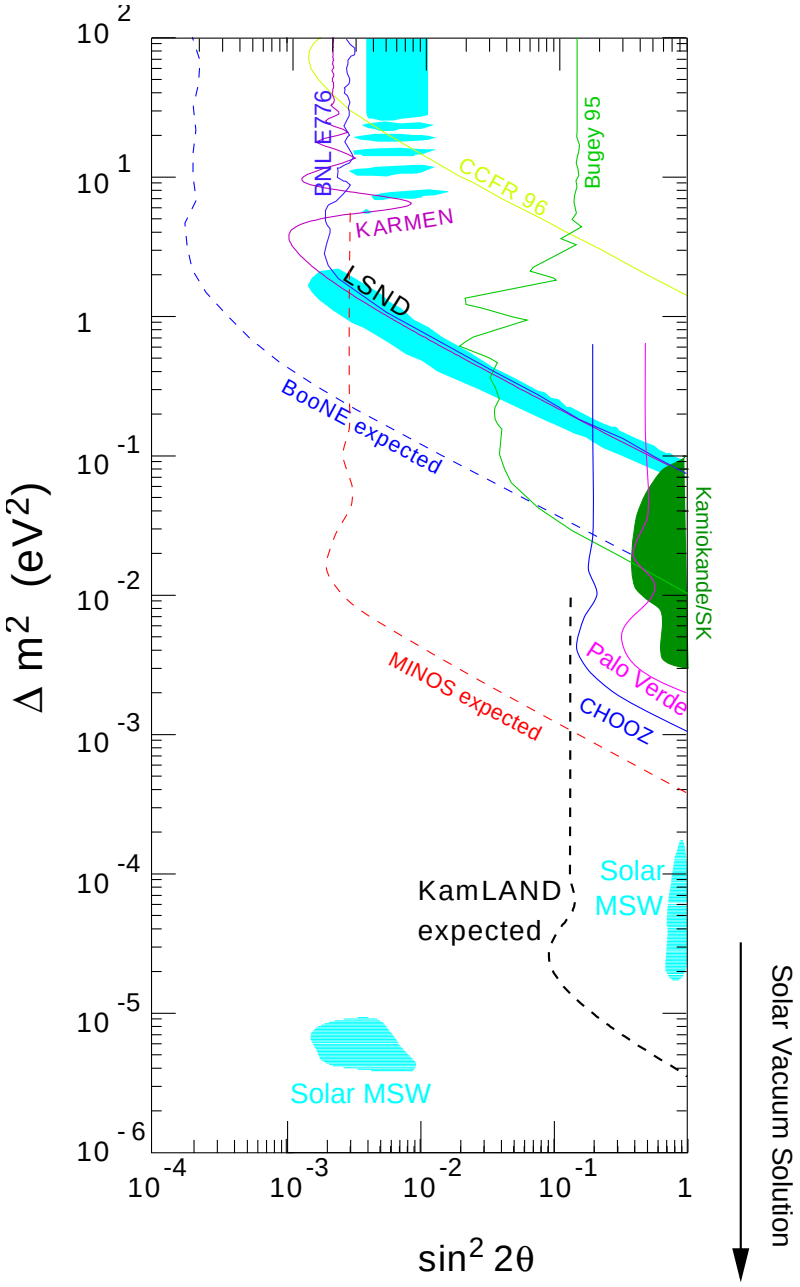

Figure 1: Phase-space for neutrino oscillations. The existing limits on $\nu_e - \nu_\mu$ are compared with current and future experiments and the regions obtained by interpreting the solar, atmospheric and LSND neutrino anomalies as due to oscillations (some of these effects are not necessarily $\nu_e - \nu_\mu$ oscillations.) The MSW mechanism is used in plotting some of the solar neutrino regions. The sensitivity of reactor experiments is the same for $\nu_e - \nu_\tau$ oscillations. Limits are at 90% CL. The new SNO result discussed in the text is not included in the figure.

solar neutrino data at the same time. In particular, oscillation solutions based on the MSW effect[11] provide several isolated islands in the Δm^2 – $\sin^2 2\theta$ plane. Two solutions correspond to $\Delta m^2 \approx 10^{-5}$ eV^2. One of them has rather small $\sin^2 2\theta \approx 10^{-2}$ (SMA) and is today somewhat disfavored by global fits to the data. The other one corresponds to essentially full mixing ($\sin^2 2\theta \geq 0.5$) and Δm^2 of 10^{-5} eV^2 to 10^{-3} eV^2 (LMA). Another solution, also for large $\sin^2 2\theta$, corresponds to 10^{-7} eV^2 (LOW). Yet another possibility, involving oscillations in vacuum, has much smaller $\Delta m^2 \approx 10^{-10}$ eV^2 and large mixing angle $\sin^2 2\theta \approx 1$, and is currently also disfavored .

The second set of measurements that is today regarded as the most compelling evidence for neutrino oscillations is the "atmospheric neutrino anomaly" [1, 4]. Primary cosmic rays impinging on the nitrogen and oxygen nuclei at the top of the earth's atmosphere produce mostly pions, which subsequently decay via $\pi \to \mu\nu_\mu, \mu \to \mathrm{e}\nu_\mathrm{e}\nu_\mu$. The resulting atmospheric neutrinos therefore are expected to follow the $\nu_\mu : \nu_\mathrm{e} = 2 : 1$ ratio, which is essentially independent of the details of the complicated process that created them. In addition, in an underground detector, one can deduce the direction of the incoming neutrinos from the direction of the leptons (e and μ) created by the charged current interactions, at least at high enough energies. Again, one is reasonably confident that this zenith angle distribution can be accurately predicted. If the ν_μ and/or ν_e neutrinos oscillate, one expects deviations from the 2:1 ratio mentioned above. Also, since the zenith angle is simply related to the neutrino path length, one expects deviations from the expected zenith angle dependence of the lepton yield.

Both signatures of neutrino oscillations were in fact observed. The ν_μ/ν_e ratio is noticeably smaller, only about 60% of the expected value of 2. This result has been confirmed in four detectors thus far. The anomalous zenith angle dependence was first observed in Kamiokande, and has been now confirmed, with much better statistical significance, by Super-Kamiokande. If these effects indeed signify neutrino oscillations (and we do not have another viable explanation) then the corresponding mixing angle is large, $\sin^2 2\theta \approx 1$. The value of the mass parameter Δm^2 remains uncertain, but is clearly in the range 10^{-2} - 10^{-4} eV^2. Super-Kamiokande data, along with the results from the Chooz [12] and Palo Verde [13] reactor experiments clearly prefer the scenario involving $\nu_\mu \to \nu_\tau$ oscillations.

Finally, the only indication for oscillations involving artificially-made neutrinos comes from the LSND experiment which finds evidence for the $\bar{\nu}_\mu \to \bar{\nu}_\mathrm{e}$ and, with more limited statistics, also for $\nu_\mu \to \nu_\mathrm{e}$ [2]. The former channel uses neutrinos from the pion and muon decay at rest, with energies less than $m_\mu/2$. The latter channel uses neutrinos from the pion decay in flight which have somewhat higher energies. These are appearance experiments; the observed signal should be absent if neutrinos do not oscillate. The well determined quantity is the oscillation probability, which has the value of about 3×10^{-3}. This result has not been independently confirmed but it is not contradicted by other evidence either.

A summary of the evidence for oscillations is given in Figure 1. While the tentative conclusion is that oscillations do occur and, hence, neutrino masses are non-zero,

only the parameter $\Delta m^2 = m_i^2 - m_j^2$ is measured with oscillations so that we have no knowledge of the individual mass values. Only a kinematics measurement or the observation of neutrino-less double beta decay can elucidate the actual mass scale.

Drastically different mass scenarios are still allowed by data. Theoretical models span a large range, from the degenerate case where the mass differences are small when compared to the absolute mass scale [6], to the hierarchical, where mass differences are of the same order as the masses themselves. While the neutrino mass scale is unknown, the present oscillation data lead rather naturally to neutrino masses in the range $0.01 < m_\nu < 1$eV as shown recently [7]. Moreover, the atmospheric neutrinos which provide the most convincing evidence for neutrino oscillation to date, allow one to establish model independent *lower* limit of ~ 55 meV ($\simeq \sqrt{3 \times 10^{-3}\text{eV}^2}$, the most probable Δm^2 for atmospheric neutrinos) for the mass of at least one massive neutrino, thus defining the relevant mass scale. It is this mass range that we propose to explore.

2.2 Cosmological implications

Neutrino masses also play a remarkable role in cosmology. If neutrinos are stable, or at least have lifetimes longer than the age of the Universe ($\simeq 10^{10}$yr), one confidently expects the existence of a primordial neutrino sea, analogous to the well established 2.7 K background microwave radiation. The corresponding temperature of today's sea of neutrinos is 1.9 K, colder than in the case of photons. The number density of such relic neutrinos is expected to be ~ 300 cm^{-3} including all neutrino flavors. If neutrinos are massive, then enough mass could be contained in the neutrino sea to account for at least part of the "dark matter" in the universe. Since the critical energy (or mass) density of the universe is $\rho_c \sim 5$ keVcm^{-3}, neutrino masses of up to 15 eV (mass average over the three flavors) would explain most of the mass in the universe. However, it is generally accepted that, for a number of reasons, neutrinos alone cannot contribute more than a fraction of the critical density. In fact, recent analysis of the cosmic structure formation [14] yields an upper limit of ~ 0.6 eV for the case degenerate neutrinos. Thus, the experimental observation of neutrino masses between a few meV and one (or a few) eV would have very significant consequences for cosmology and astrophysics.

2.3 Double-beta decay

Double beta decay is the transition between a nucleus of charge Z and mass number A (with A and Z both even) and one of same mass number but charge $Z + 2$. Here we will limit ourselves to a review of results and problems, while a more complete treatment is given in several review articles [15].

In its basic form ($2\nu\beta\beta$) double beta decay can be regarded as two β^- decays

happening simultaneously, so that the process

$$(Z, A) \rightarrow (Z + 2, A) + \mathrm{e}_1^- + \mathrm{e}_2^- + \bar{\nu}_{\mathrm{e}1} + \bar{\nu}_{\mathrm{e}2} \tag{5}$$

produces four leptons in the final state. While this second-order process is a rather standard manifestation of nuclear physics, its rate is expected to be proportional to $(G_F \cos\theta_C)^4$ where G_F is the Fermi coupling constant and θ_C the Cabibbo angle. Hence double beta decay would be an unobservably small correction to regular beta decay if it was not for a peculiarity in the nuclear mass function that in some cases renders the first order process (regular β^- decay) energetically disallowed. As shown in Figure 2 (for the case of A=136), odd-odd and even-even nuclei are arranged on two different mass parabolae because of the different value of the pairing term in the nuclear binding energy. While the direct β transition (^{136}Xe $\rightarrow^{136}$ Cs) is now forbidden, the double-β process is here energetically possible. Although this situation

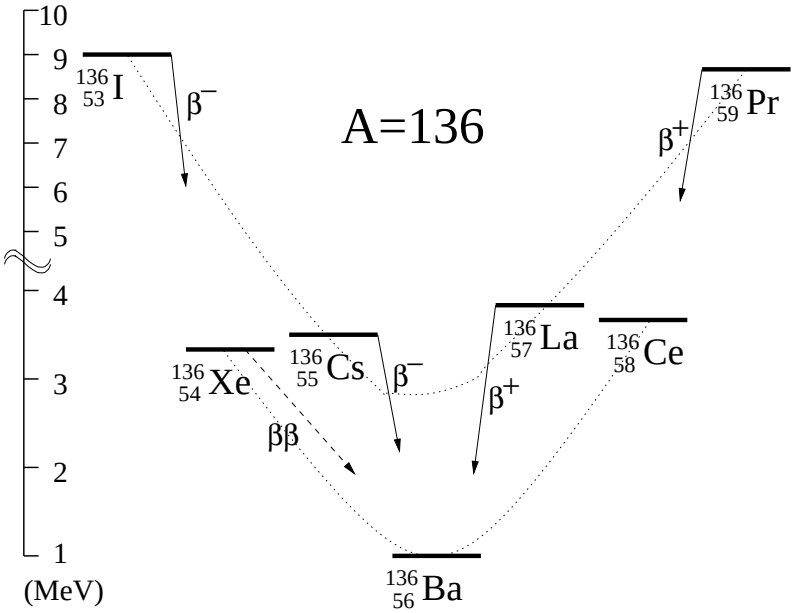

Figure 2: Simplified atomic mass scheme for nuclei with A=136. The parabolae connecting the odd-odd and even-even nuclei are shown. While ^{136}Xe is stable for ordinary β^- decay, it can decay into ^{136}Ba by a double-beta process.

is rather common, only in 11 cases the kinetic energy available to the leptons (Q) is larger than 2 MeV so that the hypothetical double-β decay can be observed in good experimental conditions.

$2\nu\beta\beta$ decay has been observed in some 11 different isotopes and the half life measured can be used to verify nuclear structure models in the presence of second order weak processes. Calculations in general agree quite well with measurements.

As illustrated in Figure 3 a different kind of double beta decay ($0\nu\beta\beta$) involving no neutrinos in the final state may occur if lepton number is not a conserved quantity *and* neutrinos have non-zero mass. Here the requirement of lepton number non-conservation derives from the fact that the anti-neutrino emitted in A has to be identical to a neutrino in order to be re-absorbed in B (Majorana neutrino). Furthermore, since weak interactions only couple to left-handed states, the neutrino has to have a mass in order not to be an eigenstate of helicity.

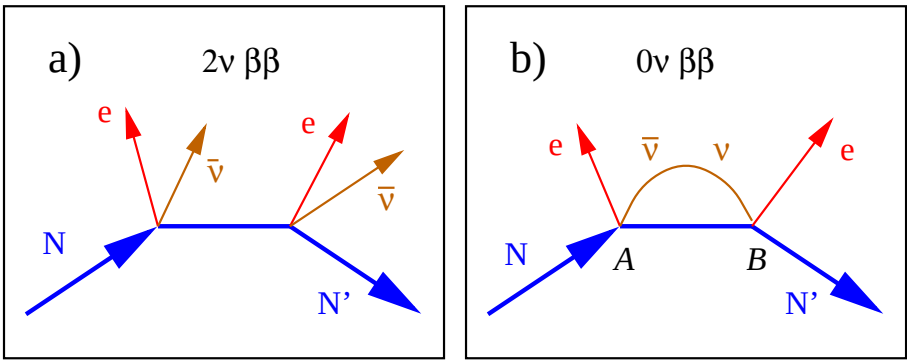

Figure 3: Feynman graphs relative to: a) 2-neutrino and (b) 0-neutrino double-beta decay processes.

In addition, if the lepton number non-conservation is due to a mechanism of spontaneous symmetry breaking, double beta decay could occur as

$$(Z, A) \rightarrow (Z + 2, A) + e_1^- + e_2^- + \chi \tag{6}$$

where the particle χ (Majoron) is the Goldstone boson of the lepton number symmetry breaking. In all models χ is a weakly interacting particle that cannot be detected.

While it is known [16] that new, exotic particles can be replaced for the neutrino in Figure 3b and produce $0\nu\beta\beta$, it is in general true that the observation of $0\nu\beta\beta$ would imply the discovery of previously unknown physics. Indeed the connection between neutrino masses or, in general, new physics beyond the "standard model" and the existence of $0\nu\beta\beta$ drives the interest for this process.

The decays $2\nu\beta\beta$, $0\nu\beta\beta$ and $\chi\beta\beta$ experimentally can only be differentiated from each other from the spectrum of the total electron energy in the final state as shown in Figure 4.

If the $0\nu\beta\beta$ process occurs, then the *effective* Majorana neutrino mass $\langle m_\nu \rangle$ is related to the half-life $T_{1/2}^{0\nu\beta\beta}$ as:

$$\langle m_\nu \rangle^2 = (T_{1/2}^{0\nu\beta\beta} G^{0\nu\beta\beta}(E_0, Z) |M_{GT}^{0\nu\beta\beta} - \frac{g_V^2}{g_A^2} M_F^{0\nu\beta\beta}|^2)^{-1} \tag{7}$$

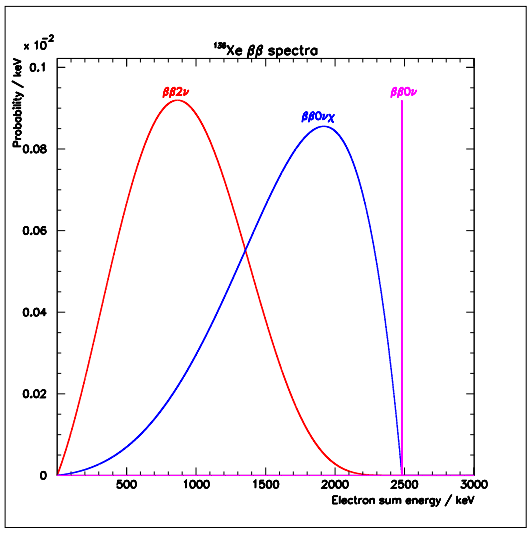

Figure 4: Spectra for the sum of electron energies in the final states for the three different ^{136}Xe $\beta\beta$ decay modes considered in the text. The relative amplitudes of the different curves are arbitrary. While the exact positions of the peaks in the spectra differ for various isotopes, the general features are obviously common to all $\beta\beta$ emitters.

where $G^{0\nu\beta\beta}(E_0, Z)$ is a known phase space factor depending on the end-point energy E_0 and the nuclear charge Z, and $M_{GT}^{0\nu\beta\beta}$ and $M_F^{0\nu\beta\beta}$ are the Gamow-Teller and Fermi nuclear matrix elements for the process. Here we have defined

$$\langle m_\nu \rangle = \sum_i m_i U_{ei}^2 \tag{8}$$

U being the mixing matrix in the lepton sector and m_i the masses of the individual Majorana neutrinos. Hence $0\nu\beta\beta$ decay is sensitive to the masses of all neutrino flavors, provided that the mixing angles are non-negligible. (Note that in Eq. (8) the mixing angles appear as simple, not absolute, squares. Hence the so-called Majorana phases, signifying the properties of the mass eigenstates under CP, can cause cancellations in the incoherent sum in Eq. (8).)

From Equation 7 we find that the sensitivity to neutrino masses improves only with the square root of the sensitivity in half-life. Difficulties in the nuclear models used to calculate the matrix elements gives some uncertainty to the value of $\langle m_\nu \rangle$ derived for a particular $T_{1/2}^{0\nu\beta\beta}$.

It was recently shown [7] that the present data on oscillations leads very naturally to effective masses in the range 0.01eV $< \langle m_\nu \rangle <$ 1eV. In this proposal we show that this range of masses can be explored in the next several years with a large ^{136}Xe double beta decay experiment. The measurement of a non-zero $\langle m_\nu \rangle$, together with the oscillation data available, will then allow us to start the exploration of the

CP phase in the lepton sector of the CKM matrix and will provide crucial input to cosmology.

It is important to realize that a positive signal for $0\nu\beta\beta$ or $\chi\beta\beta$ decay would represent a substantial breakthrough in physics and hence will require a high degree of confidence in the data. A meaningful experiment needs to use a technique able to produce solid and reliable results with negligible effects due to backgrounds.

2.4 Present status of $0\nu\beta\beta$ decay searches

Several experiments have been carried-out in the past searching for $0\nu\beta\beta$ decay and to date no positive result has been reported.

Since the phase-space factor $G^{0\nu\beta\beta}$ is a steep function of the end-point energy ($G^{0\nu\beta\beta} \simeq (E_0^5/30 - 2E_0^2/3 + E_0 - 2/5)$ in the Primakoff-Rosen approximation), in practice only isotopes with the largest Q values can be used in a competitive fashion. In addition a likely candidate should have reasonable natural isotopic abundance. Finally, competitive experiments are generally performed in relatively deep underground sites where cosmic-ray background is reduced. In Table 1 we list the $\beta\beta$ decay candidates with $Q > 2$ MeV along with their isotopic abundance and phase space factors for $0\nu\beta\beta$ and $2\nu\beta\beta$ decays.

$\beta\beta$ decay candidate	Q (MeV)	Isot. Abund. (%)	$1/G^{2\nu\beta\beta}$ (yr)	$1/G^{0\nu\beta\beta}$ (yr)
^{48}Ca $\rightarrow^{48}$ Ti	4.271	0.187	2.52×10^{16}	4.10×10^{24}
^{76}Ge $\rightarrow^{76}$ Se	2.040	7.8	7.66×10^{18}	4.09×10^{25}
^{82}Se $\rightarrow^{82}$ Kr	2.995	9.2	2.30×10^{17}	9.27×10^{24}
^{96}Zr $\rightarrow^{96}$ Mo	3.350	2.8	5.19×10^{16}	4.46×10^{24}
^{100}Mo $\rightarrow^{100}$ Ru	3.034	9.6	1.06×10^{17}	5.70×10^{24}
^{110}Pd $\rightarrow^{110}$ Cd	2.013	11.8	2.51×10^{18}	1.86×10^{25}
^{116}Cd $\rightarrow^{116}$ Sn	2.802	7.5	1.25×10^{17}	5.28×10^{24}
^{124}Sn $\rightarrow^{124}$ Te	2.228	5.64	5.93×10^{17}	9.48×10^{24}
^{130}Te $\rightarrow^{130}$ Xe	2.533	34.5	2.08×10^{17}	5.89×10^{24}
^{136}Xe $\rightarrow^{136}$ Ba	2.479	8.9	2.07×10^{17}	5.52×10^{24}
^{150}Nd $\rightarrow^{150}$ Sm	3.367	5.6	8.41×10^{15}	1.25×10^{24}

Table 1: Double beta decay isotopes with $Q > 2$ MeV, from [17]. For ^{48}Ca and ^{96}Zr β decay is kinematically allowed but extremely suppressed by spin considerations.

In Table 2 we show the best sensitivity reached to date for $0\nu\beta\beta$ decay. Although several experiments have been performed in which the $0\nu\beta\beta$ source is external to the detecting apparatus, there are clear advantages in schemes where the source is in a form that can serve also as detector for the electrons. Indeed the experiments showing the best sensitivity all utilize this principle.

$\beta\beta$ decay candidate	$T_{1/2}^{0\nu\beta\beta}$	Reference
^{48}Ca	$> 9.5 \times 10^{21}$ (76% CL)	[18]
^{76}Ge*	$> 5.7 \times 10^{25}$ (90% CL)	[19]
^{82}Se	$> 2.7 \times 10^{22}$ (68% CL)	[20]
^{100}Mo	$> 5.2 \times 10^{22}$ (68% CL)	[21]
^{116}Cd	$> 2.9 \times 10^{22}$ (90% CL)	[22]
^{130}Te*	$> 5.6 \times 10^{22}$ (90% CL)	[23]
^{136}Xe*	$> 4.4 \times 10^{23}$ (90% CL)	[24]
^{150}Nd	$> 1.2 \times 10^{21}$ (90% CL)	[25]

Table 2: Recent results in $0\nu\beta\beta$ decay experiments. Isotopes marked * are discussed in some detail in the text.

We concentrate here on ^{76}Ge, ^{130}Te, and ^{136}Xe that have provided the best sensitivity to date.

$\beta\beta$ decay in ^{76}Ge had been studied using germanium diode ionization counters of very large volume. In this case the detector and the source are made of the same material and the event tagging is purely calorimetric. In recent times germanium detectors have been built out of isotopically enriched ^{76}Ge drastically improving the sensitivity. The isotopic separation and the clean condition used for a diode-quality crystal automatically provide low intrinsic detector background. The best sensitivity is achieved by the Heidelberg-Moscow experiment [19] at Gran Sasso, where detectors totaling 11 kg (86% ^{76}Ge) have been taking data for 2.6 yrs. Total exposure for the most recent reported results is 53.9 kg·y (35.5 kg·y with the pulse shape analysis). Typical energy resolutions of $FWHM \simeq 3$ keV at 2 MeV are achieved. This is the best figure obtained in any detector so far. The excellent energy resolution is particularly useful in discriminating between $0\nu\beta\beta$ (mono-energetic) and $2\nu\beta\beta$ (energy continuum). The total background observed in the detector, using the pulse shape analysis, is reported to be of 0.3 kg^{-1} yr^{-1} FWHM^{-1}. The half-life limit of 5.7×10^{25} yrs gives a neutrino mass limit of $\langle m_\nu \rangle < 0.2(0.6)$ eV using the "Quasi-Particle Random Phase Approximation" or QRPA [26] ("Shell Model" or NSM [27]) for the nuclear matrix element calculation.

^{130}Te has the big advantage of a rather large isotopic fraction in natural tellurium (34.5%). However the realization of the particle detector is in this case more exotic. A calorimetric detector is possible by observing the temperature rise due to the electron energy being deposited in a TeO_2 crystal. This is only possible at very low temperature since the heat capacity is proportional to T^3 so that in cryogenic conditions a very small energy deposition causes a detectable temperature increase. In principle the ultimate energy resolution of such detectors is superior to germanium diodes, although this has not yet been practically demonstrated in large crystals. The present

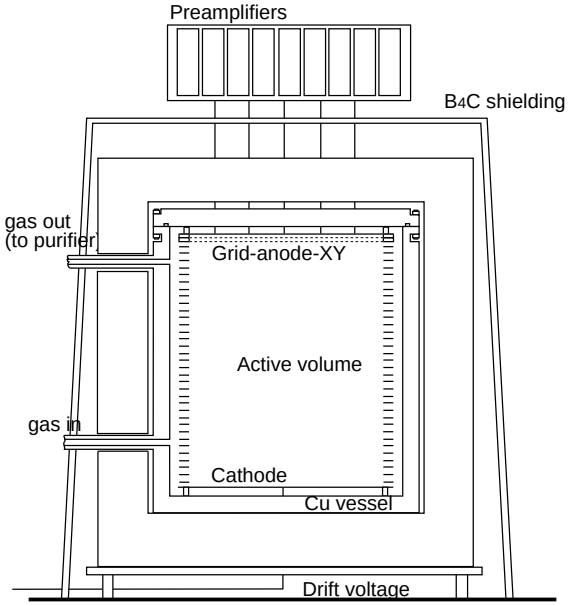

Figure 5: Scheme of the Gotthard TPC used in [24]. The total height of the active volume is 67.7 cm.

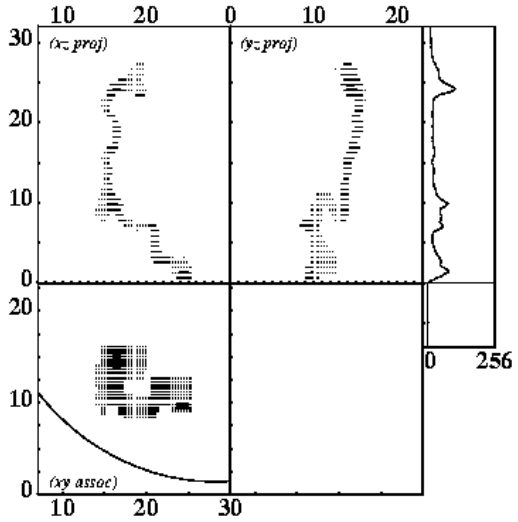

Figure 6: Electron tracks from a candidate double-beta decay event in xenon from [24]. The two main top panels show the xz and yz projections of the event, while the reconstructed xy view is given in the bottom part (dimensions are in cm). Pulse-height information is shown in the smaller panel on the right (in ADC counts). Note the higher ionization density at the end of the tracks. The circular sector in the bottom-left corner of the xy view represents the edge of the TPC.

limit [23] (Table 2) was obtained with a 20 crystals of tellurium oxide, totaling about 6.8 kg, running at a temperature of 8 mK. The detectors have a resolution $FWHM \sim$ 8 keV at 2.5 MeV and logged 0.66 kg y of ^{130}Te in the Gran Sasso Laboratory. The background reported in this case is $\sim$4 kg^{-1} yr^{-1} FWHM^{-1}. The resulting half-life limit of 1.44×10^{23} corresponds to a neutrino mass limit of $\langle m_\nu \rangle < 1.8(3.8)$ eV in the QRPA (NSM) approximation.

The search for $\beta\beta$ decay in ^{136}Xe needs substantially different techniques. Since Xe is a noble gas it is particularly advantageous to use the same gas as detecting medium in an ionization chamber. In modern times the "Time Projection Chamber" (TPC) configuration has been used, providing full spatial tracking of the electron trajectories with minimal extraneous materials in the active volume. The technique for background rejection is also quite different: while the energy resolution is not sufficient, alone, to completely suppress the background, the final event selection also uses the tracking information, showing the two-electron final state for the $\beta\beta$-decay case and only one electron from Compton scattering produced by most natural radioactivity backgrounds. The best sensitivity for ^{136}Xe has been achieved in a 5 atm TPC containing 5.3 kg of Xe enriched to 63% in ^{136}Xe operated inside the Gotthard road tunnel in Switzerland [24]. A sketch of this detector is shown in Figure 5.

The total running period was 1.5 yr and, the energy resolution was $FWHM =$ 6.6% at 1.592 MeV (105 keV). The background was 2.5 kg^{-1} yr^{-1} FWHM^{-1}. The superior tracking capability of this technique is apparent in Figure 6 where two projections ($x - z$ and $y - z$) for a double-beta decay candidate are shown. Since multiple scattering is substantial at 5 atm and no time-zero was provided in the Gotthard TPC, a two-electron event, like in the case of $\beta\beta$ decay, does not appear very different from a single-electron event produced, for instance, in a Compton scattering from background γs. In both cases multiple scattering of the low-energy track(s) is the dominant feature and two-electron events are selected only by observing the increase of specific ionization towards the end of the track(s). The number of such high ionization "blobs" effectively counts the electrons in the event. The resulting half-life limit of 4.4×10^{23} corresponds to a neutrino mass limit of $\langle m_\nu \rangle < 2.2(5.2)$ eV in the QRPA (NSM) approximation.

3 Detector design concepts

As described earlier $0\nu\beta\beta$ decay experiments represent the most sensitive means we have to directly measure neutrino masses in a region that is extremely important for particle physics and cosmology. The most sensitive searches for $0\nu\beta\beta$ to-date have used up to about 10 kg of nearly-pure isotopic species; hence further substantial progress can only be achieved through an ambitious program where *tons* of an appropriate isotope are monitored for a relatively long time. Indeed it is legitimate to ask whether backgrounds can be reduced to a small enough level such that full use can be made of the large mass of active material. This point is essential: in a background-

free experiment the sensitivity to the half-life $T_{1/2}^{0\nu\beta\beta}$ is directly proportional to the number of nuclei N and exposure time t, so that the neutrino mass sensitivity scales as:

$$\langle m_\nu \rangle \propto 1/\sqrt{T_{1/2}^{0\nu\beta\beta}} \propto 1/\sqrt{Nt}. \tag{9}$$

However, unless some new technique is used, the small background observed in all the current experiments will increase with the mass and exposure time and become the true limiting factor of any kind of experiment. If we crudely assume that backgrounds increase linearly with Nt we would be in a regime where the sensitivity on $T_{1/2}^{0\nu\beta\beta}$ is limited by the statistical fluctuations in the background ($T_{1/2}^{0\nu\beta\beta} \propto \sqrt{Nt}/Nt$). Hence the neutrino mass sensitivity would scale only as:

$$\langle m_\nu \rangle \propto 1/\sqrt{T_{1/2}^{0\nu\beta\beta}} \propto 1/(Nt)^{1/4}. \tag{10}$$

Indeed this simple scaling only applies to backgrounds from materials that are internal to the active mass, since external backgrounds will be shielded to some degree from the larger mass. Still qualitative new means to suppress backgrounds are needed in order to utilize fully very large masses of $\beta\beta$ emitters.

^{136}Xe is an ideal isotope for this purpose since:

- it is one of the easiest isotopes to enrich;
- like argon, which is the mainstay of proportional chambers, it represents a good ionization detecting medium;
- it exhibits substantial scintillation that can be used to complement the ionization detection;
- most importantly its $\beta\beta$ decay produces a final state nucleus of ^{136}Ba that can be identified in its atomic form with powerful new techniques of high resolution optical spectroscopy;
- it has no long-lived isotopes that can be activated;
- being chemically inert it can be easily purified with different techniques involving molecular sieves, hot metal getters and electric discharges;
- being a gas at STP it can be easily transferred, so that new purification techniques or even drastically different detector designs can be easily implemented.

Hence a Xe TPC (in gaseous or liquid phase), which has produced among the smallest specific backgrounds reported to date, will be supplemented with the system of ^{136}Ba identification, adding one new degree of freedom to be used for background reduction. The Ba tagging technique was first proposed in this context in [33] and then discussed in [34]. While the size and properties of the detectors considered here are similar to

those of chambers that successfully took data for many years (see for instance [35, 36]), the Ba tagging technique, which is new to particle physics, has been commonly employed in atomic physics for the past two decades.

In this LOI we will outline two options for the design of a large detector using liquid xenon (LXe) and high-pressure gaseous xenon (GXe). These two options result in quite different tradeoffs:

- A LXe detector would be a-priori a more elegant solution, since 10-tons of xenon would be contained in a small ~ 3 m^3 container using modest cryogenics (xenon liquefies at 165 K at 1 atm). However, as it will be explained later, it is presently not clear if the energy resolution that can be attained in the liquid phase would be sufficient to separate the $0\nu\beta\beta$ from the $2\nu\beta\beta$ mode. In order to perform laser tagging the Ba-atoms produced in the decays will have to be extracted from the liquid where collisional line broadening is probably too severe and the Rayleigh scattering of the laser beams would produce substantial stray light. Once extracted from LXe Ba-atoms could be studied in low pressure Xe gas, probably allowing to detect not only the chemical species but also the isotope, hence providing one further constraint.

- A GXe detector would certainly have enough energy resolution to allow for $0\nu\beta\beta$ to $2\nu\beta\beta$ separation up to the best sensitivity (largest fiducial mass) contemplated here. However in order to contain 10 tons of xenon one would have to use a very large volume pressurized detector. While the parameters considered here are technically achievable, it is rather clear that the additional complication would result in higher costs both for the detector and for the underground cavities and shielding required. The lower density in the gas-phase would provide long enough electron tracks to use some form of tracking to further reject background. But the main difference in a gas-phase detector would regard the implementation of the Ba tagging. While on one hand Ba extraction would probably be unfeasible it is likely that laser beams could be directly steered on to the region of the chamber where the decay occurred. Mundane –but very real– issues involving the light scattering in the detector would have to be addressed. In this version of the detector no isotope identification would be done by the laser tagging since the background gas would substantially broaden the atomic lines.

The R&D program described in the following is intended to answer these questions and provide input in the final detector design. In addition to the issues raised above it is not completely clear what are the tradeoffs of the two options in terms of internal radioactivity contamination. Experience shows that in this arena predictions are not very robust, and it is best to rely on actual tests. While contamination data for a GXe detector can be readily derived by the Gotthard double beta decay experiment, we are planning, as part of the R&D, to build a 100 kg LXe prototype that will address contamination issues as wall as many other points discussed below.

3.1 A high pressure Xe gas TPC Concept

The concept of a 10 atm gas TPC is shown in Figure 7. The primary requirements for the TPC modules are:

1) Large size and high pressure in order not only to have a few modules, but also to have the highest possible efficiency (fully contained events) and self shielding from backgrounds produced by external materials. Indeed the concept of a TPC is ideal here because of the little extraneous materials present inside the detector;

2) Good energy resolution in order to distinguish $0\nu\beta\beta$ from $2\nu\beta\beta$ decays;

3) Sufficient spatial resolution in three dimensions (low diffusion and ability to provide the time when the event occurred (T0));

4) Low background environment;

5) Ability to neutralize Ba^{++} to Ba^{+} (or Ba^{0});

6) Ba^{+} (or Ba^{0}) lifetime in the chamber 10 s $\lesssim \tau_{Ba} \lesssim$ 1 hour, where the lower limit derives from the need to identify spectroscopically the Ba atom or ion and the upper limit insures that only a few Ba atoms or ions are present in the chamber at any given time;

7) Ability to perform laser spectroscopy within its volume.

While some of these requirements are in partial conflict with each other (for instance position resolution is best for small-sized chambers) we find a gas TPC of about 40 m^3 to be a good tradeoff between all these requirements. At 10 atm and 20°C xenon has a density of 57 g/l, so that the chamber would contain 2.3 tons of gas. A full size 10 ton detector would be composed of four identical modules. At this density 1.25 MeV electrons range in 16.1 cm so that tracking can substantially help in background suppression, as shown by the successful operation of the Gotthard TPC. We note here that a single module of 40 m^3 could contain 10 tons of gas if operated at 30 atm. While in this condition the power of the tracking would be substantially affected, the pressure vessel would still be within technical feasibility, similar to the one of large bubble chambers or to the casing of large solid propeller rockets. Some advantages may derive from operating the chamber below room temperature since in this way the same density could be obtained at a lower pressure.

As illustrated in Figure 7 the TPC volume would be defined by an acrylic cylinder of 3.2 m diameter and 5 m total length. The cylinder will also serve as rigid mechanical structure defining the position and distance of the different TPC components. A very thin cathode plane, formed by a copper coated Kapton membrane, will be placed halfway along the cylinder, effectively dividing the system into two drift volumes and two

anode readout planes, as customary in large TPC design (see for instance [29, 35]). At a drift field of 1 kV/cm each gap will require a total voltage of 250 kV, which is still within the reach of commercial power supplies [30].

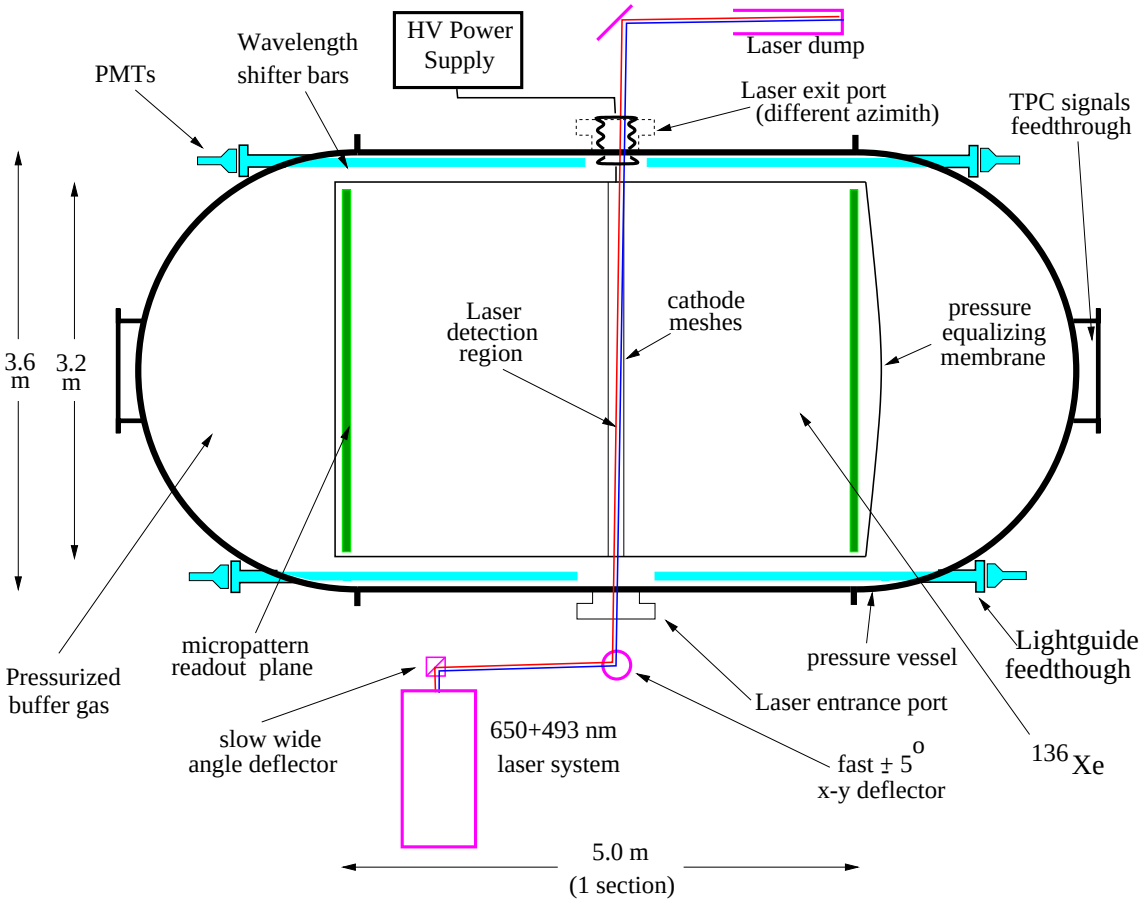

Figure 7: Conceptual layout of the high pressure gas detector. The TPC is surrounded by a layer of gas that electrically insulates it from and transfers the pressure to the external pressure vessel. Wavelength shifting bars couple the scintillation and Ba-fluorescence light to external PMTs. Ba-ions are drifted to a central plane where the laser spectroscopy is performed. Alternatively the lasers can be directly steered to the decay positions. A rather elaborate system of windows, baffles and mirrors will be needed in order to feed and remove the laser beam from the chamber without causing undue scattering of light into the photomultipliers. All laser beam handling parts will be located away from the cathode plane which is biased at about -250 kV respect to ground. Not shown in the drawing is the external γ-ray shielding. Materials used for the construction of the chamber itself, such as acrylic, Teflon, Kapton and copper will be intrinsically clean, while the pressure vessel will be built out of specially selected carbon steel. Low activity glass will be used for the photomultiplier tubes. Depending upon the choice of pressure several TPC modules may be installed in a single, longer pressure vessel.

Field shaping electrodes will be installed on one of the surfaces of the acrylic cylinder either by mounting solid copper rings or by depositing copper strips. The resistive chain will be located outside the cylinder. Given the size of the end-plates we do not favor at this time the use of wires for the signal amplification and readout. Rather we are considering the use of some type of micro-pattern detector (MPD, see e.g. [31]). The high pressure will be contained by a separate vessel isolated from the cathode plane by pressurized gas. The acrylic cylinder will be closed at one end by a solid acrylic plate and at the other by a flexible membrane (or bellows) made out of a thin plastic film. This membrane would confine the xenon to the TPC active volume while absorbing small pressure differences between the xenon and the buffer gas. An inert gas at the same pressure as the Xe would fill the volume between the pressure vessel and the TPC proper. Optical readout of the Xe scintillation and the Ba^+ fluorescence would be achieved with wavelength shifter bars, contained inside the pressure vessel, coupled to PMTs at atmospheric pressure. This arrangement minimizes the transverse dimensions of the vessel, reduces the radioactivity from the glass in the vicinity of the Xe and keeps the PMTs outside of the high pressure environment. Large acceptance ($\approx 50\%$) can be achieved in this fashion. Assuming the inert gas to be nitrogen we would need 10 cm between the central cathode edge and the closest photomultiplier in order to hold, at 10 atm, the 250 kV. A thinner gas layer would be required at higher pressure. The use of heavier gases (like CBr_4) that would also provide some shielding for external radioactivity is currently under consideration.

In order to withstand a pressure P the vessel has to have a thickness of $t = Pr/2\sigma$ where σ is the strength of the material. We use $\sigma = 1300$ atm (having applied a safety factor of 2 to the figure for carbon steel) and obtain a thickness of 8.4 mm for $r = 180$ cm and $P = 10$ atm or 2.9 cm at $P = 35$ atm. Depending upon operating pressure, relative ease of installation at the site and cost we can conceive of using carbon steel or high strength composite structure for the pressure vessel. Carbon fiber cylinders of similar size and pressure rated to 75 atm are commonly produced as casings for large solid-fuel rockets. A relatively thin, non structural OFHC copper inner liner may be desirable to define a clean, low activity and metallic inner surface. A special system with double o-rings and the middle volume purged by a vacuum pump will be used at the flanges in order to exclude the possibility that leaks could result in loss of ^{136}Xe .

The spectroscopic tagging would happen in a central plane where the Ba-ions would be drifted like shown in the figure, or by steering directly the laser beams onto the target regions identified by the TPC trigger. The entire laser transport and steering system will have to be engineered so that the beam(s) would enter the chamber and exit to a dump through a low-loss system. This task, particularly non-trivial in the second case, would be essential to minimize the light scattering onto the photomultipliers.

3.2 A liquid TPC Concept

The primary motivation for choosing the liquid phase of xenon for the detecting medium is the high density of the medium, thereby reducing the volume of the detector. The modest size of a liquid detector is highly desirable for placing the detector in a mine, which inherently limits the size. On the other hand the high density of the liquid phase makes the laser detection in the bulk rather hard. Hence we are developing a system capable of extracting single barium ions from a particular location in the liquid into low pressure xenon vapor. This is conceptually similar to the extraction of Ar of Ge atom from the radiochemical solar neutrino experiments except that the extraction is done mechanically, in quasi-real-time conditions.

A conceptual scheme for realizing a full scale (> 1 ton) liquid xenon TPC is shown in Figure 8. This particular concept consists of a toroidal cryostat for the xenon, although a rectangular version would also be possible. The inner wall at large radius would function as a cathode, and on the inner wall at small radius would be an anode segmented in both azimuth (ϕ) and in height (the z direction). Close to the anode at larger radius would be a highly uniform grid. Ionization produced by the beta electrons would be drifted to the anodes and collected, and positional information regarding the ionization event would be provided by the anode segmentation (for reconstruction of ϕ and z), and by the measured drift time (for reconstruction of the radial position r). The bottom of the vessel would be provided with closely spaced UV-transparent windows through which a series of photomultiplier tubes would collect scintillation light. The signals from the photomultipliers would provide both a timing signal for the electron drift time measurement as well as additional calorimetric information which would supplement the ionization signal.

A polar-coordinate robotic arm would be used to position an electrostatic barium ion extraction probe to the location of the ionization event. The probe would then deliver the barium to an ion trap, which in this design is integrated into the horizontal robot arm, for spectroscopic identification by the laser resonance technique.

3.3 Barium spectroscopy and atom tagging

As described above, extrapolating the radioactive backgrounds observed in any of the present generation $\beta\beta$ detectors, much larger experiments are predicted to be background dominated. Indeed large volumes provide additional self-shielding, and small improvements can be obtained by careful workers. However it is clear that only qualitatively new tools can provide the improvement of performance needed for a substantial and worthwhile new effort in the search for $0\nu\beta\beta$ decay. The use, for the first time, of highly selective laser detection of the final atomic state would provide an entirely new process for the rejection of radioactive backgrounds.

Single atom laser detection methods are new to particle physics but have become widely used in atomic physics in the last twenty years, and were recognized in the 1990 Nobel Prize award [37] to Dehmelt, Paul, and Ramsey. Resonant laser detection

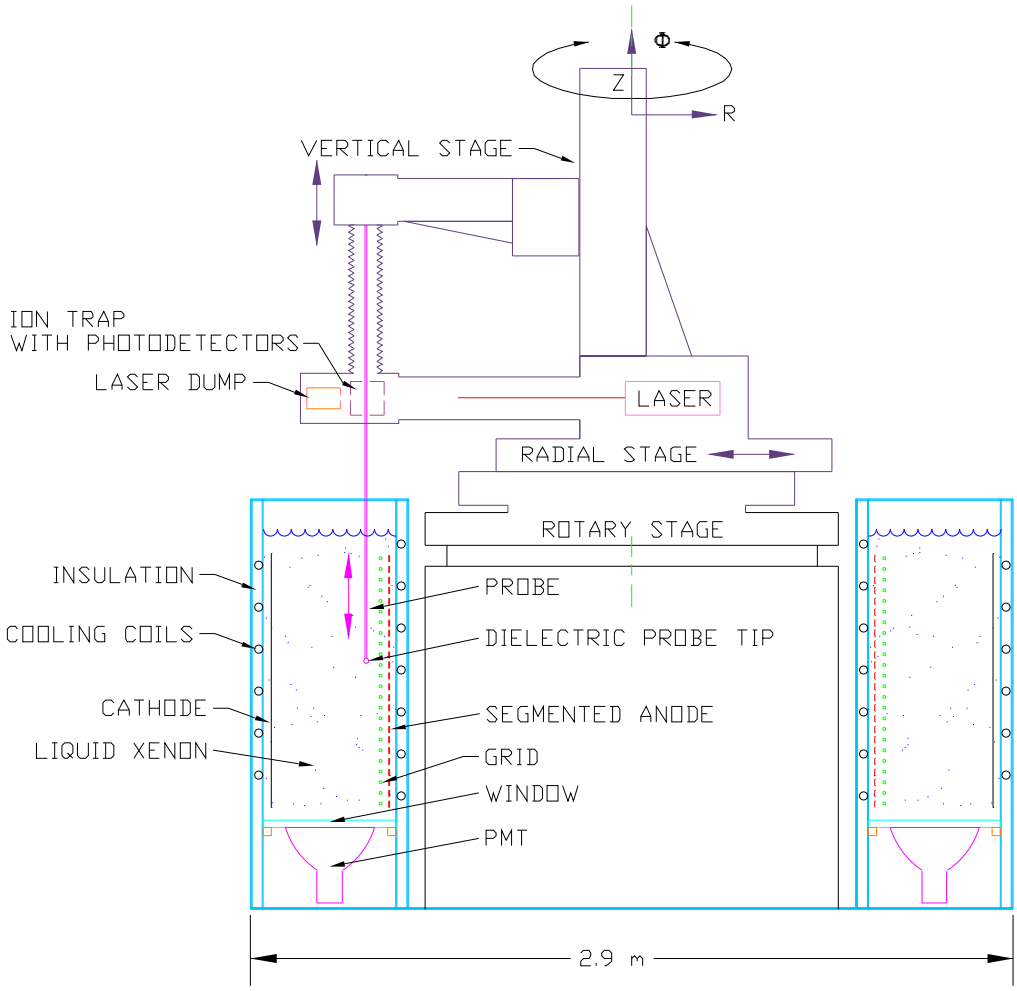

Figure 8: Conceptual design of the LXe detector.

is both highly sensitive, yielding $\geq 10^7$ photons per second from a single atom, and highly selective, since this large scattering rate only occurs over a narrow band of frequencies which are unique to each element. Moreover, the atomic physics community has had twenty years experience in observing single barium atoms, since it was the first atom to be observed [38] in 1978 and in some ways is the easiest atom to detect.

In the following we will review the history of recent atomic physics work on single barium atoms, consider the effect of high pressure xenon on the laser detection process and outline the laser apparatus required to observe resonant scattering in a large-volume, high-pressure TPC.

3.3.1 Laser Detection of Single Atoms in Atomic Physics

Single atom laser detection techniques have become widely used in atomic physics in the last few years. Single barium ions were first observed in 1978 by Dehmelt [38] and collaborators using a radio frequency quadrupole trap and laser cooling. These traps use electromagnetic forces to suspend the ion in an ultra-high vacuum while a laser is used to cool the ion to temperatures of a few millikelvin. Laser cooling is nowadays common in atomic physics and was recognized in the 1997 Nobel prize award to Chu, Cohen-Tannoudji and Phillips. The cold ion is confined to a region a few nanometers from the center of the trap where it is free from Doppler broadening and collision effects so that it behaves like an ideal single atom previously considered only in gedanken-experiments. The study of single trapped atoms has provided order-of-magnitude improvements in frequency standards as well as qualitatively new work in quantum optics, quantum computation, chaos, and Wigner crystallization. At present, three groups are operating ion traps using Ba^+, while about a dozen others are studying single trapped ions of other elements, including calcium, strontium, magnesium, and beryllium.

The level structure of the $^{136}Ba^+$ ion is shown in Figure 9. It is typical of an alkali atom, which has a single valence electron outside a closed shell. There is a strong allowed transition at 493 nm between the $6^2S_{1/2}$ ground state and the first excited state $6^2P_{1/2}$ and a weaker transition between the $6^2P_{1/2}$ and the meta-stable $5^4D_{3/2}$ separated by 650 nm. The 493 nm transition has a spontaneous lifetime of 8 ns and, when saturated, will radiate 6×10^7 photons/s. The branching ratio of decay into the D (S) state is 30% (70%).

3.3.2 Barium Detection in High Pressure Xenon

The primary difference between the single atom work done previously and this experiment is that here the Ba^+ ion is observed in a buffer gas (xenon) at different pressures. This is in contrast with the ion trap work which limits the buffer gas pressures to 10^{-8} atm. The high pressure xenon has two effects: first, it obviates the need for a trap since diffusion in the dense gas is sufficient to confine the atoms for long enough time to obtain a signal; second, it pressure broadens the optical transitions,

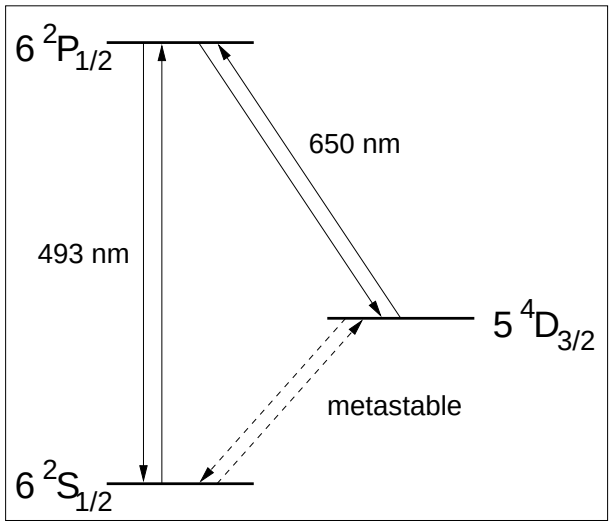

Figure 9: Atomic level scheme for Ba^+ ions.

which increases the laser power required. While the similar case of line broadening of barium in He and Ar at pressures up to ≈ 0.5 atm can be found in literature [39], measurements will be needed to characterize precisely the system for the parameters of interest to us.

It is clear from the discussion above that, depending upon the xenon phase chosen for the detector, the requirements on the laser tagging system change drastically. In particular a LXe detector with Ba extraction into a small chamber where low pressure Xe is present can result in spectroscopic lines that are narrow compared to the isotope shifts, hence allowing one to confirm that the isotope produced is the relatively rare ^{136}Ba (7.8% in natural barium).

Here we will discuss the issues related to the spectroscopy in the more challenging case of 10 atm pressure background pressure. This already requires an extrapolation of some parameters from well understood regimes, and even higher pressures can only be reliably estimated once the results of the R&D proposed will be available.

Diffusion can be understood as a random walk problem. The mean free path ℓ in xenon at 10 atm is 1 nm and the mean time between collisions is $\tau = 4$ ps. The total distance L traveled in a time t will then be $L = \ell\sqrt{n}$ where $n = t/\tau$. Therefore the barium ion will diffuse only $\simeq 0.4$ mm in 1 s while during this time it will scatter $\geq 10^7$ photons.

Pressure broadening can be understood as a simple application of the Fourier Theorem. The mean time between collisions of 4 ps is 2000 times shorter than the 8 ns spontaneous emission lifetime. Each collision randomizes the phase of the atomic dipole, and therefore reduces the time over which the optical frequency is defined. The pressure broadened line-width is therefore 2000 times greater than the natural

line-width of 20 MHz. The pressure of 10 atm corresponds to a 40 GHz full-width-half-maximum (FWHM) Lorentzian line-shape function.

The most significant effect of pressure broadening is that it increases the laser power required to achieve the maximum photon scattering rate of 6×10^7 photons/s, called the "saturation" laser intensity $I_{\rm sat}$. The pressure broadened line-width is thus a key experimental parameter since it sets the overall laser power and thus defines the type of laser technology required. For most atomic systems, $I_{\rm sat}$ is proportional to the pressure, so that 10 atm of Xe will require a laser intensity of ~ 10 W/cm^2. For each event the TPC will conservatively provide a region of interest of 3×3 cm^2 so that the laser power needed would be ~ 100 W. CW lasers of this power level are not available commercially, so that one must either operate below saturation where the scattering rate is $\propto I/I_{\rm sat}$, or use a more tightly focussed scanning beam, or use pulsed lasers. One should note that although previous single atom experiments have operated in the saturated regime, they have also used small solid angles ($\approx 10^{-3}$) for the photon detection. The much larger solid angle coverage (≈ 0.1) contemplated here can therefore compensate for the lower photon emission rate expected in a non-saturated regime. If saturated operation is desired a synchronously-pumped mode-locked pulsed laser can be used which generates a train of high power picosecond pulses with a repetition rate of ≈ 100 MHz. Because of the 8 ns lifetime of the Ba^+ fluorescence, the 100 MHz repetition rate will lead to quasi-CW photon emission which will approximate the maximum saturated value. Because the value of $I_{\rm sat}$ determines the overall design of the detection system, it is important to measure the pressure-broadening parameters of Ba^+ in a small-scale preliminary experiment. In the density-matrix theory of laser-atom interactions, this comprises a measurement of relaxation times for the diagonal and off-diagonal density matrix elements, called T_1 and T_2 respectively, which completely determine the response of the atom to laser light.

Apart from these effects one may worry that the physical size of the chamber in which we want to detect single atoms is very large, even in the case of the flat, central detection region. Three additional methods that can be used to mitigate the effect of direct light scattering in the PMTs:

- The first method uses the meta-stable D state as a bottleneck in an optical pumping cycle. The result is that the blue 493 nm light can be switched on and off by modulating the 650 nm red light. This gives an unmistakable signature that the light comes from the specific atomic species sought. The applicability of this method depends on the effect of the xenon buffer gas on the D-state lifetime, which is not known at present but will be investigated experimentally.

- The second method uses an electro-optic frequency modulator to shift the frequency of the 493 nm laser light without changing its intensity. Current devices can shift the frequency by 20 GHz in about 500 ns. Modulating the laser frequency in this fashion, the presence of the right atomic species would then be

signaled by a modulated count rate, which would distinguish it from simple scattered light.

- The third method can be used in conjunction with pulsed laser excitation, and utilizes the 8 ns spontaneous emission lifetime of the barium atoms to discriminate between resonant laser excitation and scattered background light. The scattered light will have the time-dependence of the picosecond excitation pulse, while emission from Ba^+ will decay exponentially with an 8 ns lifetime. A histogram of the photon arrival time will therefore provide another discriminant for the detection of Ba^+.

The use of one of the above methods or a combination of them together with careful masking should make the atom detection, even for a very large volume, very reliable.

3.3.3 Laser Detection System

The laser detection system for the gaseous Xe detector option consists of three major parts: the laser source, the beam pointing system, and the photomultiplier detection array.

Double beta decay of ^{136}Xe produces the doubly ionized isotope $^{136}Ba^{++}$, which cannot be easily detected using current laser technology since its transitions lie below 150 nm where efficient laser sources do not exist. However both the singly charged ion Ba^+ and the neutral atom Ba are suitable candidates for laser detection. Ba^+ has a strong dipole allowed transition from the 6S to the 6P state at 493 nm while neutral Ba has a similar transition at 554 nm. Both transitions lie in the visible part of the spectrum where powerful lasers and detectors with high quantum efficiency are available. We will discuss the case of Ba^+ in the following.

The trigger for the laser system is provided by the TPC detecting two electron-type events. It takes several hundred microseconds for the ionization trails produced by the electrons to drift to the TPC gain region and collection pads or wires. The signals amplified by the front-end electronics are then fed to a trigger processor that produces an estimate of the location of the potential double beta decay candidate within 100 μs. A beam pointing system can utilize two classes of devices: galvanometer driven mirrors, which have millisecond response time and can swing by any angles, and acousto-optic beam deflectors, which have microsecond response time but more modest (few-degrees) deflections. Depending on the exact topology of the chamber a combination of the two might be necessary. Driftin the ions to a pancake-shaped central detection region would simplify the laser pointing system. The same array wavelength shifters and PMTs discussed in the context of the xenon scintillation light detection can also be used to detect the Ba^+ de-excitation photons of 493 nm.

Resonant excitation of the Ba^+ ions will produce $\geq 10^7$ photons per second, which is sufficient to identify the atom in a fraction of a second. Assuming conservatively

10% collection coverage and a 1% combined figure for quantum efficiency and wavelength shifter conversion yield the detected resonant count rate will be >10 kHz. As discussed, non-resonant scattered light from the laser beams can be suppressed by a lock-in scheme which either frequency-modulates the lasers off the atomic resonance or intermodulates the fluorescence using an optical pumping bottleneck, as described previously. We expect to be able to reduce the background from scattered light to negligible levels. We note that an atom observation period of 1 s is extremely conservative: as discussed above the barium ion will diffuse $< 1\mu$m in 1 ms, so if needed it is reasonable to imagine extending the observation period to several seconds in order to enhance the signal-to-noise ratio.

3.4 Expected backgrounds and Detector Performance

The experiment will have to be located in an underground site in order to provide shielding against cosmic radiation. We expect to install the detector either at the National Underground Science Facility that has been proposed for the Homestake site [40] or at the DoE WIPP site near Carlsbad NM. Here we summarize the conclusions of background estimates performed for the WIPP site and discussed in detail in [41]. We believe these results to be quite conservative since the WIPP overburden is only $\simeq$ 2000 mwe (meter water equivalent). A placement at Homestake will provide extra shielding against cosmic rays. On the other hand the WIPP site is known to be substantially lower in γ radiation from U and Th decays and in Rn concentration in the air.

The $\simeq$ 2000 mwe overburden will reduce the cosmic ray muon flux to $\simeq 2 \times 10^{-3}\mathrm{m}^{-2}\mathrm{s}^{-1}$, corresponding to less than 0.1 Hz through the detector. Muons have a very distinctive signature and indeed were observed and rejected by the Gotthard group [28] based on track length, limited scattering (high energy) and specific ionization. The last two features provide good discrimination even for tracks that clip a small corner of the chamber. The online trigger processor will be able to analyze and reject most muon tracks without activating the laser Ba-tagging system. Based on simple geometrical considerations we expect the laser beacon to be activated by muon tracks less than once per hour.

Some background will be caused by neutrons produced by muon spallation in the structures (rock and other materials) outside the detector. These fast neutrons enter the detector with some efficiency and produce spallation reactions on the xenon, carbon and hydrogen nuclei contained in the TPC. While the original muon and the neutron trail go undetected the spallation processes provide very distinct high ionization, short tracks that are easy to distinguish and reject even at trigger level. We tentatively conclude that at the depth considered, an active veto counter may not be needed (as found by the Gotthard group [28]), although it would be rather trivial to implement.

More serious is the background from natural radioactivity, either produced outside

the TPC (mainly by the rock or concrete), or inside (mainly ^{222}Rn and, possibly, ^{85}Kr and ^{42}Ar). Our preliminary estimates indicate that the external shielding alone should be sufficient for the experiment at least at the WIPP site. External backgrounds from the rock and concrete, substantially more severe at Homestake, could be attenuated by a ∼25 cm thick lead or steel enclosure. Additionally, cleaner shielding could be provided, if needed, by a layer of de-ionized water or mineral oil located inside the pressure vessel. Such a layer could readily add a further factor of $\simeq$ 1000 of attenuation to 1.2 MeV γs (1 m of thickness) and moderate external neutrons.

In the following we conservatively assume that the TPC itself (without Ba-tagging system) will have the same specific rate of mis-identified background as the Gotthard experiment, and we rely on Ba-tagging to keep the backgrounds from radioactivity to a negligible level for very large exposures. This hypothesis is conservative since the larger volume of our TPC provides better self shielding for the radiation produced externally. Internal backgrounds will be limited by careful choice of construction materials (essentially only copper, acrylic, Teflon and polyamide films) and by removing contaminants from the xenon.

We assume the energy resolution to be no worse than the $\sigma_E = 2.8\%$ (obtained at Gotthard) and since in addition to the total charge, also the scintillation light will be collected[32] this assumption should be conservative. As we will discuss below sub-1% resolutions have been obtained in high pressure xenon gas. We will also give some sort of "asymptotic sensitivity" that will be obtained with the more aggressive resolution of 2% and a very long data-taking with a 10 ton detector (100 ton yr exposure).

From the size and geometry of the chamber we obtain an efficiency for fully contained events of 70%. We note that there will be no residual Ba^+ in the detector since barium is a reactive metal with a negligible vapor pressure at room temperature. Any barium produced will drift in the electric field to the cathode walls where it will form a chemical bond and disappear.

It is interesting to note that for very large quantities of material the background on $0\nu\beta\beta$ decay from the well known $2\nu\beta\beta$ mode becomes important. As already remarked this "background" is obviously not suppressed by the laser tagging methods, and, since its only distinctive feature is the electron energy spectrum (see Figure 4), kinematical reconstruction is the only effective tool.

Before discussing this last step of data reduction we briefly discuss the $2\nu\beta\beta$ sample that this project would produce. Assuming that the $2\nu\beta\beta$ half-life is 8.5×10^{20} yr [42] we will already have 8.6×10^6 decays (at 70% reconstruction efficiency) after the first phase of the experiment (5 yr ton). This number of events can be compared to the ∼20,000 $2\nu\beta\beta$ events observed in ^{76}Ge [43], and ∼1500 events in ^{100}Mo and ^{116}Cd [44]. The project described here will increase, as a "by-product", the world sample of $2\nu\beta\beta$ decay events by about three orders of magnitude. The combination of TPC and laser tagging will enable full kinematic reconstruction of the events (as was done in [44] for the ^{100}Mo and ^{116}Cd cases), so that we will be able to measure not only the sum energy spectrum, but also determine the vertex position, and therefore

Isotope and Reference	Total Mass (kg)	Enrich. grade (%)	Det. eff. (%)	Meas. time (yr)	Bkgd.	$T_{1/2}^{0\nu\beta\beta}$ (yr)	$\langle m_\nu \rangle$ (eV) QRPA	NSM
^{76}Ge [17]	11	86	75	2.2	0.3	5.7×10^{25}	0.2	0.6
^{136}Xe [22]	3.3	63	22	1.47	2.5	4.4×10^{23}	2.2	5.2
^{130}Te [21]		34.5				5.6×10^{22}	2.9	6.1
^{136}Xe projected (for $\sigma_E/E = 2.8\%$)	1000	65	70	5	0^*+ 1.8 events	8.3×10^{26}	0.051	0.14
^{136}Xe projected (for $\sigma_E/E = 2.0\%$)	10000	65	70	10	0^*+ 5.5 events	1.3×10^{28}	0.013	0.037

Table 3: Comparison of the best present double-beta decay experiments and the project described here. The technique of Ba^+ tagging will reduce the background, given in units of kg^{-1} yr^{-1} $FWHM^{-1}$ if not noted otherwise, to the level necessary to fully utilize the large mass of isotopic species. All other experimental parameters are assumed to be the same as in the Gotthard experiment. We list here, together, the case of an initial detector with 1 ton of ^{136}Xe and the final results possible with 10 tons of ^{136}Xe and a very long (10 years) data-taking period. The quantities marked with * are radioactivity backgrounds that are assumed to be negligible as discussed in the text. In addition the background from mis-identified $2\nu\beta\beta$ decays is also shown in total events in each exposure using the asymmetric analysis interval described in the text.

observe the single electron spectra and the two-electron angular correlations. This will enable us to study in detail the mechanism of the $2\nu\beta\beta$ decay and check for deviations from the pure Gamow-Teller decay, checking, for example, effects of weak magnetism-induced terms.

Moreover, with this unprecedented statistics of events reconstructed with high quality one will be able to search for the neutrinoless decay with Majoron emission, which, as shown in Figure 4, would manifest itself as a small deformation of the $2\nu\beta\beta$ continuum spectrum.

While the $2\nu\beta\beta$ mode is interesting on its own right, a reasonable resolution on the total energy measurement will remove it effectively and hence obtain a background-free sample for the $0\nu\beta\beta$ mode. We select events in the interval $I_+ = [Q_{\beta\beta}, Q_{\beta\beta} + 2\sigma_E]$ (where, as discussed, $\sigma_E = 2.8\%$ in the first phase while later $\sigma_E = 2\%$). The asymmetric interval is chosen to maximize the $0\nu\beta\beta$ relative to $2\nu\beta\beta$, which has a steeply decreasing spectrum in this region. We then compute the number of $2\nu\beta\beta$ decay events left in each case. For the first phase we have 1.8 $2\nu\beta\beta$ events left, while 5.5 events are left in the 100 yr ton data-sample. These backgrounds are then statistically subtracted using the $2\nu\beta\beta$ rate prediction from other regions of the energy spectrum. It should be remarked that on one hand this procedure relies on a good understanding of the resolution function, while, on the other, our total number of $0\nu\beta\beta$ events is conservatively estimated using the relatively short half-life predicted in [42]. The result in terms of sensitivities to the $0\nu\beta\beta$ half-life and neutrino masses are shown in Table 3 together with the present best data. The loss in efficiency due to

the asymmetric cut (and to the tails beyond 2σ) are taken into account in the table as appropriate.

In summary this experiment at its various stages will allow us to explore neutrino masses in the interesting range 10 meV - 1 eV, providing a unique opportunity for discoveries in particle physics and cosmology.

4 Detector R&D Program

R&D being performed towards a detector concentrates on the following points:

- Characterization of the Ba^+ optical spectroscopy in presence of background Xe gas (Stanford, IBM).
- Study of ultra-purification techniques for Xe, both in terms of electronegative impurities and radioactive contaminants (SLAC. Alabama).
- Study of the ultimate energy resolution in liquid Xe with scintillation light and charge readout (Stanford, SLAC, ITEP)
- Development of a device to extract single Ba ions from liquid to gas phase in Xe (SLAC).
- Measurements of backgrounds at WIPP and Homestake and radiological characterization of construction materials (Alabama).
- Development of electron multiplier planes for a gas detector (Neuchatel).
- Design and construction of a 100 kg prototype without Ba-tagging to be deployed filled with ^{136}Xe in the next one year (SLAC, Stanford)

In this section we will briefly discuss each of the above items.

4.1 Ba^+ optical spectroscopy

The detailed design of the laser system depends on the results of the preliminary experiments to study pressure broadening and charge exchange, as discussed above. The charge exchange experiment will determine whether to use Ba^+ or Ba for the laser detection. While both cases are feasible, in the case of Ba^+ the laser technology involved is simpler. The pressure broadening experiment will determine the required laser power, which in turn will influence the choice of CW or pulsed laser excitation. Since the experiment must operate with minimal attendance for many months, a solid state laser system is preferred. With present technology the most reliable system would be a frequency-doubled laser diode, as such devices are non-critical and commercially available at 986 nm for doubling to 493 nm for Ba^+.

We have built an apparatus to verify experimentally that single atoms of Ba^+ can be detected by laser excitation in the presence of high-pressure xenon gas. The apparatus, schematically shown in Figure 10, consists of an ion trap of about 5 mm linear dimensions, which can operate at pressures from the UHV range to a few atmospheres. Single Ba^+ ions as well as clouds of up to 100 ions are trapped initially at 10^{-9} Torr and xenon gas is then gradually added while observing the fluorescence. There should be no change in the intensity of resonance fluorescence as the xenon pressure is increased from 10^{-9} Torr to 10^{-2} Torr and any loss of signal will indicate the presence of impurities in the gas. Above about 10 mTorr pressure broadening will dominate the response and the atomic transition will become weaker and broader. By measuring the intensity as a function of detuning from resonance we will be able to determine the cross-sections for both phase-interrupting collisions (parameterized by the off-diagonal relaxation time $T2$) and energy-quenching collisions (the diagonal relaxation time T1). These two coefficients (together with a corresponding pair for the D state) completely determine the effect of the xenon gas on the laser-atom interactions. In addition, the diffusion coefficients can be measured by observing the movement of the ion when the rf trap is turned off. This apparatus will also let us test more complicated methods of driving single ions, for example, the quasi-CW excitation proposed above.

We will then excite a resonance transition in the trapped ions using low-power, frequency-stabilized laser diodes and detect the ions using a combination of photodetectors and lock-in techniques.

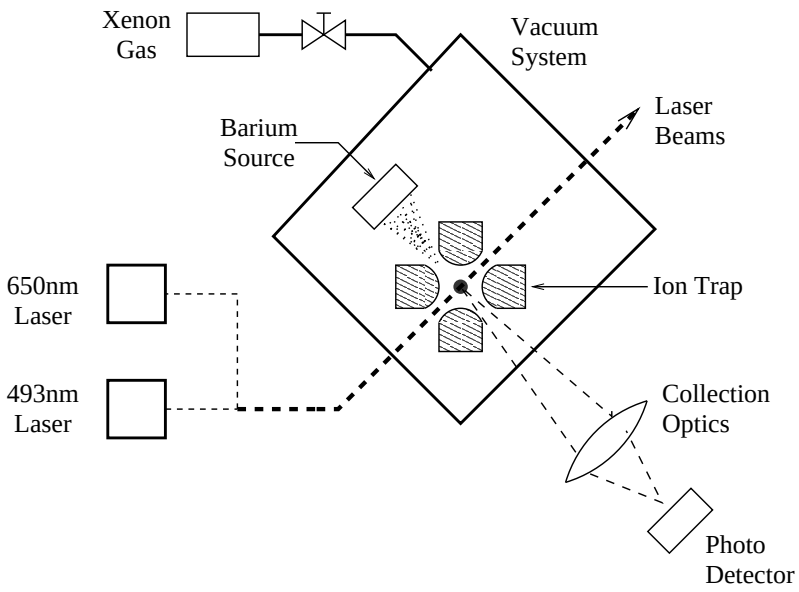

Figure 10: Schematic overview of the single atom fluorescence spectroscopy experiment.

The setup is shown in Figure 11. The RF ion trap is on the top-right of the figure inside the UHV system. Mounted with the trap is a neutral barium source and a 500 eV, 1 μA electron gun. The electron gun, barium source, and trap are mounted so that the electrons ionize neutral barium in the trapping volume without obstructing optical access to the atoms. The trap itself consists of three electrodes mounted on insulating ceramic with ≈ 2 mm of optical clearance.

Two laser frequencies are required to detect Ba^+ via fluorescence spectroscopy, 650 nm and 493 nm. For both frequencies, we use External-Cavity Diode Lasers (ECDL) to obtain the required frequency tuning capabilities and narrow linewidth characteristics. An ECDL uses a diffraction grating mounted on a Piezo-Electric Transducer (PZT) to provide frequency-dependent optical feedback into a commercial diode laser. Although ECDL's are capable of providing line-widths below 100 kHz and continuous tuning over 100's of GHz, our lasers only need to achieve line-widths on the order of 50 MHz and a tuning range up to 20 GHz. To fulfill these requirements, we use commercially available, inexpensive components to provide a stable current source and to temperature control the laser. The diffraction grating and PZT are attached to a custom mount and electronic feedback is provided using custom electronics. The laser's frequency spectrum is analyzed using a scanning Fabry-Perot interferometer, and the absolute laser frequency is determined with the aid of a Burleigh Wavemeter. Since no commercial diodes exist at 493 nm, we double a 986 nm diode in a single pass non-linear crystal waveguide. The laser systems with their diagnostics are visible on the optical table in Figure 11.

Primary detection of the fluorescence photons for our test setup is accomplished with a microscope either directly or by installing a miniaturized PMT at the place of the eyepiece. A chopper wheel and lock-in amplifier allow for the enhancement of the signal for some types of measurements.

We are also testing a fully electrical ion pickup system that will allow us to simultaneously detect both Ba^+ and Ba^{++} for clouds of hundreds of ions. In this way we will be able to measure the ++ to + neutralization times under different conditions.

4.2 Xe purification techniques

The technology for purification of noble gases, particularly argon and xenon, has been well developed [56]. There are at least two basic techniques: distillation and adsorption of impurities on chemically active surfaces. The latter has several variants: oxysorb filters, high temperature zirconium filters, and clean titanium dust generated by a spark discharge in the apparatus [57] . Two other obvious requirements are that the apparatus be constructed of clean materials and that an appropriate purity monitor be integral with the apparatus.

We have chosen to build a first apparatus that permits distillation and adsorption in a commercial zirconium filter. The apparatus is shown schematically in Figure 12. The apparatus is scaled to handle batches of 3 kg of xenon or less. The batches

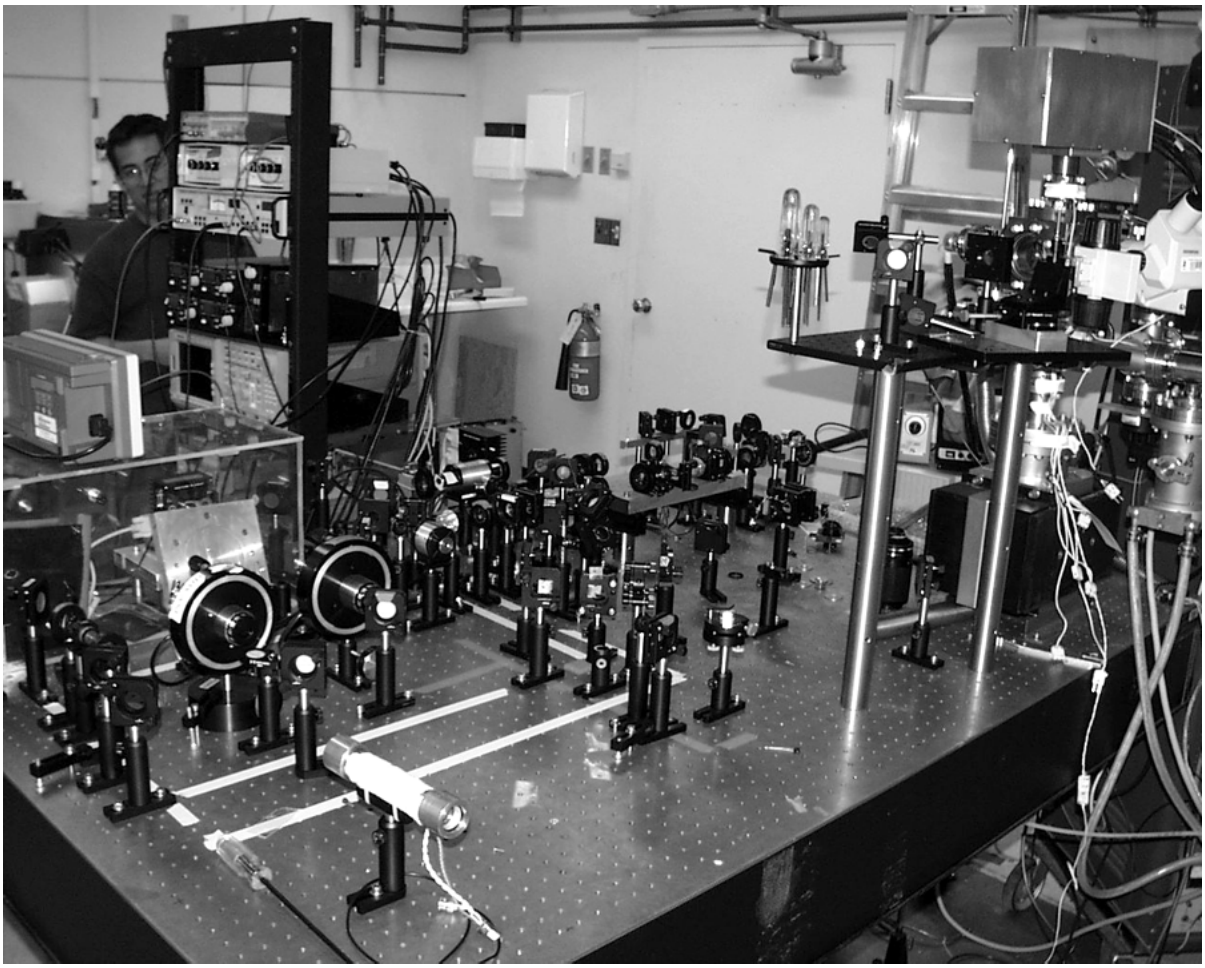

Figure 11: Ba spectroscopy laboratory.

may be recycled until the desired purity (or exhaustion) is reached. Note that the bottles may be used for storing the xenon (as a liquid with the bottle cooled by liquid nitrogen, or as a gas). There is an residual gas analyzer (RGA) with a range of 300 AMU and about 1 AMU resolution capable of evaluating (high) impurity levels, measuring isotopic composition of enriched xenon, and measuring krypton at better than 1 ppm levels. Krypton is chemically inert, so can only be removed by the isotopic enrichment process or distillation.

The apparatus is all metal and bakeable to 150 C. It is pumped by oil free turbopumps and an ion pump. Xenon purity is monitored by an electron lifetime drift cell. Ionization electrons from an alpha source are drifted in an electric field region adjustable from about 10 V/cm to about 1000 V/cm. The charge is measured separately as it enters and exits the drift region. This charge ratio divided by the drift time is a measure of the electron loss and the xenon purity.

Figure 12: Xenon purifier.

4.3 Ultimate energy resolution in LXe

As discussed above the possibility of performing the experiment in liquid phase is very attractive. One of the main issues to resolve to assess the feasibility of this option is whether the energy resolution at 2.4 MeV is sufficient to allow a clean separation of the $0\nu\beta\beta$ decay from the $2\nu\beta\beta$ background. While the best resolution obtained in a LXe ionization chamber is only $\sigma = 2.5\%$ at 570 keV [45], extremely good energy resolution has been obtained in high pressure xenon gas [46]. Indeed the result quoted in this last work $\sigma = 0.94\%$ at 122 keV is similar to what obtainable in semiconductor detectors and very close to the limit given by the excitation statistics. Although some possible explanations of why is the resolution in liquid so much worse than expected have been put forward (see for instance the discussion in [45]), none of these explanations is completely satisfactory and the poor resolution is LXe remains somewhat of a puzzle. In general it is understood that the large scintillation yield in xenon 64000 photons/MeV with no electric field, reduced to approximately 26000 photons/MeV in a 1 kV/cm electric field needs to be included in the picture if the energy resolution is to be understood. As documented by many authors the light yield decreases as the ionization yield increases with increasing electric field in the detector. This effect is qualitatively understood since the electric field separate charges that are then collected, preventing recombination that is generally associated with scintillation. Unfortunately it is not trivial to detect with good acceptance scintillation light (peaked at 175 nm) and ionization at the same time. Indeed, all

LXe detectors that have been built to-date employ scintillation light only as a trigger and have very poor solid angle coverage. Yet some measurements performed in a small detector [47] seemed to reveal that an *event by event* anti-correlation exist between the scintillation and the ionization yield, so that a substantial gain in resolution can be obtained by adding for each event scintillation and ionization signals with some appropriate weighting. Unfortunately these papers were concerned with energies with are much higher than the ones of interest here. In addition the energy deposit was produced with an intense, low-energy electron gun, hence obtaining a very high ionization density.

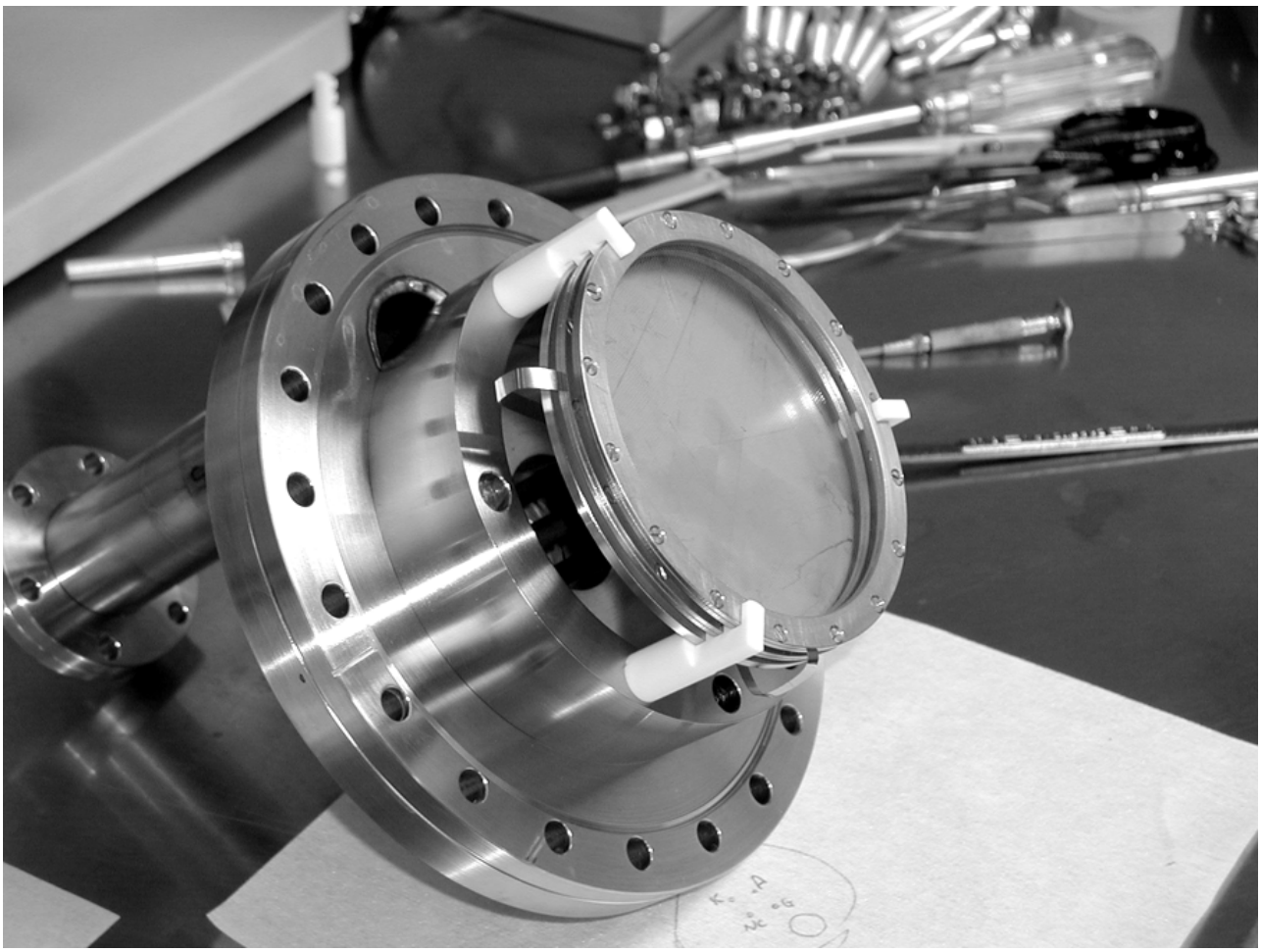

Figure 13: 1 l liquid xenon chamber to study energy resolution.

In our R&D program we have built a small (1 l liquid) chamber to study these effects at one or few MeV with electron-type ionization density. The chamber, shown in Figure 13 is designed in a pancake shape so that good scintillation light collection

can be obtained together with good ionization collection. The chamber is cooled by immersion in a bath of 3M HFE7100 cooled at $\sim -100°$C by a LN2 loop. HFE7100 is a non-flammable fluid engineered for very broad liquid phase that may be used to cool a detector where good light readout will require large windows with poor thermal conductance. The energy resolution test chamber is being commissioned at the time of writing. The performance of wavelength shifters in LXe will also be investigated in this test chamber.

4.4 Ba^+ extraction

One of the technical challenges of the measurement strategy of identifying the Ba ion is to get it to an environment suitable for the spectroscopy measurement. In the liquid xenon scenario, the present strategy is to extract the ion and move it to a low pressure test chamber for identification. More specifically, the liquid TPC would locate the ion to a few mm or better. A robot arm would insert a probe into the xenon close to the ion. The probe tip is thought of as a conducting surface covered with a dielectric. A negative potential on the tip would attract the ion to the dielectric surface and hold it during extraction from the liquid. The release of the ion is more problematic due to the details of the dielectric surface fields. It is possible that with a good dielectric (e.g. diamond) reversal of the field will eject the ion. Another possibility is that the probe tip might be coated with solid xenon. Upon removal of the probe from the liquid, combining evaporation of the xenon from the probe tip with the reversed field might eject the ion.

Needless to say, this technique must be demonstrated early in the R&D phase. We are building a test cell to explore this strategy, but rather than work with Ba which is difficult to detect (before the spectroscopy cell exists !), we are using ^{220}Ra, which is detectable through its decay chain and is chemically similar to Ba. The cell is shown schematically in Figure 14. The ^{230}U source (half-life 20.8 days) is plated onto one of the lower electrodes. The ^{230}U decays to ^{230}Th (half-life 30.6 minutes), which decays to ^{222}Ra (half-life 38 seconds) plus an α. This decay sends some Ra ions into the liquid xenon. The ^{222}Ra goes through rapid α decays (^{222}Ra $\rightarrow$ ^{218}Rn $\rightarrow$ ^{214}Po $\rightarrow$ ^{210}Pb) and this distinct decay signature is used to count the Ra ions.

The probe picks up Ra ions from the liquid and withdraws to a counting station where surface barrier detectors can see the Ra^{222} α decay chain. The probe also can be withdrawn further to a station where the field can be reversed (and other expulsion strategies studied) and the Ra ions removed. The probe then returns to the counting station to confirm that the ions are gone or measure the amount remaining on the probe.

This cell is in the last stages of detailed design and component procurement is underway. Preliminary results are expected around the end of the calendar year.

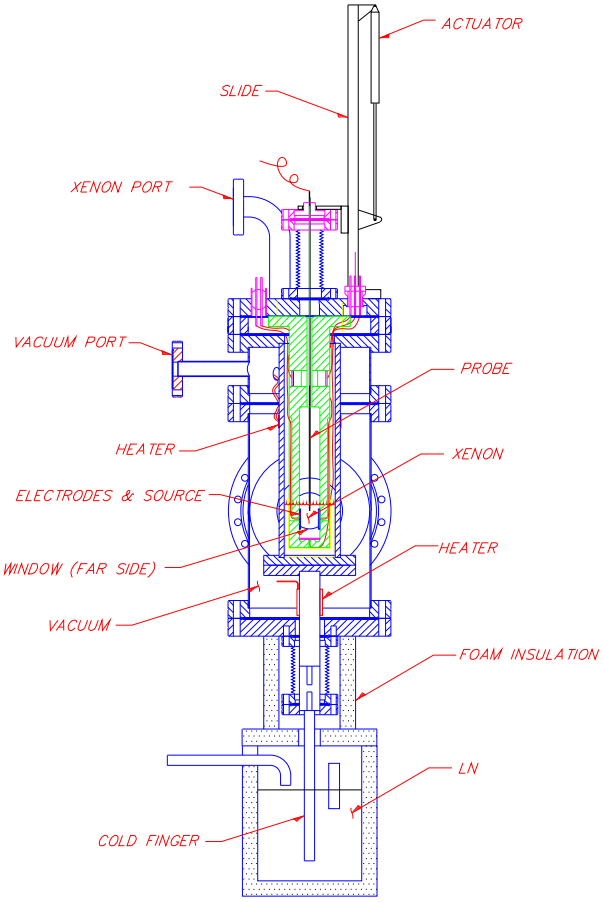

Figure 14: Schematic drawing of the ion manipulation cell.

4.5 Radioactivity Control

Although the Ba tagging feature of EXO will greatly enhance our robustness against background, a tight control of radioactive isotopes in EXO construction materials will be essential. We are planning to use different techniques in the material screening process. Our prime tool will be low background gamma ray spectroscopy. At the University of Alabama we are operating a shielded Ge detector which can be used for this work. It is equipped with a simple cosmic ray veto comprised of plastic scintillator paddles. We are planning to upgrade this veto system to provide 4π-coverage. Detection limits on the order of *mBq/kg* for bulk materials can be achieved with this device. The passive Pb-Cu shield is large enough so it may also accommodate secondary detectors which might be used to enhance our sensitivity by employing coincidence counting.

The Alabama group is also planning to use Neutron Activation Analysis for materials which are suited for this technique. This work will naturally follow from the experience gained by screening for U and Th content materials to be used in the KamLAND experiment. With the proper pre-concentration we have achieved a sensitivity of about 10^{-14} g/g for U/Th. We have established a working relation with the research reactor facilities operated at Oak Ridge National Laboratory and at the Massachusetts Institute of Technology, where we perform long term exposures (>10 h) at the highest available fluxes. The group has setup a clean room to perform pre-activation sample preparations without introduction of trace contaminations. All necessary facilities and licenses to perform post-activation radio chemistry are already in place.

The Alabama group has also been engaged in environmental measurement at WIPP. We have measured the cosmic ray muon flux and the radioactivity content at possible locations for EXO. Similar measurements can be repeated at Homestake.

4.6 Initial analysis of a ^{136}Xe sample.

A first sample of 20 l STP of xenon enriched to 90% in the 136 isotope was received in June 2001 from the Krasnoyarsk plant in Russia. A preliminary analysis of the sample was performed using an RGA that is part of the xenon handling system described in section 4.3. In Fig. 15 we show an example of mass spectrum from the enriched xenon. The peaks around 136 amu are accompanied by doubly-ionized Xe peaks around 72 amu. The peaks at lower masses are due to vacuum contaminations not discussed here.

The measured ^{136}Xe abundance of 89.5% well matches what specified by the production plant (90.3%). A peak from ^{134}Xe is clearly visible (10.4%) abundance, while the isotope 132 can be measured at 8^{-4} level. These values, along with trace amounts of the isotopes 129 and 131 are found to be in good agreement with the specifications from the factory.

The contamination from krypton is an important parameter since about a part in

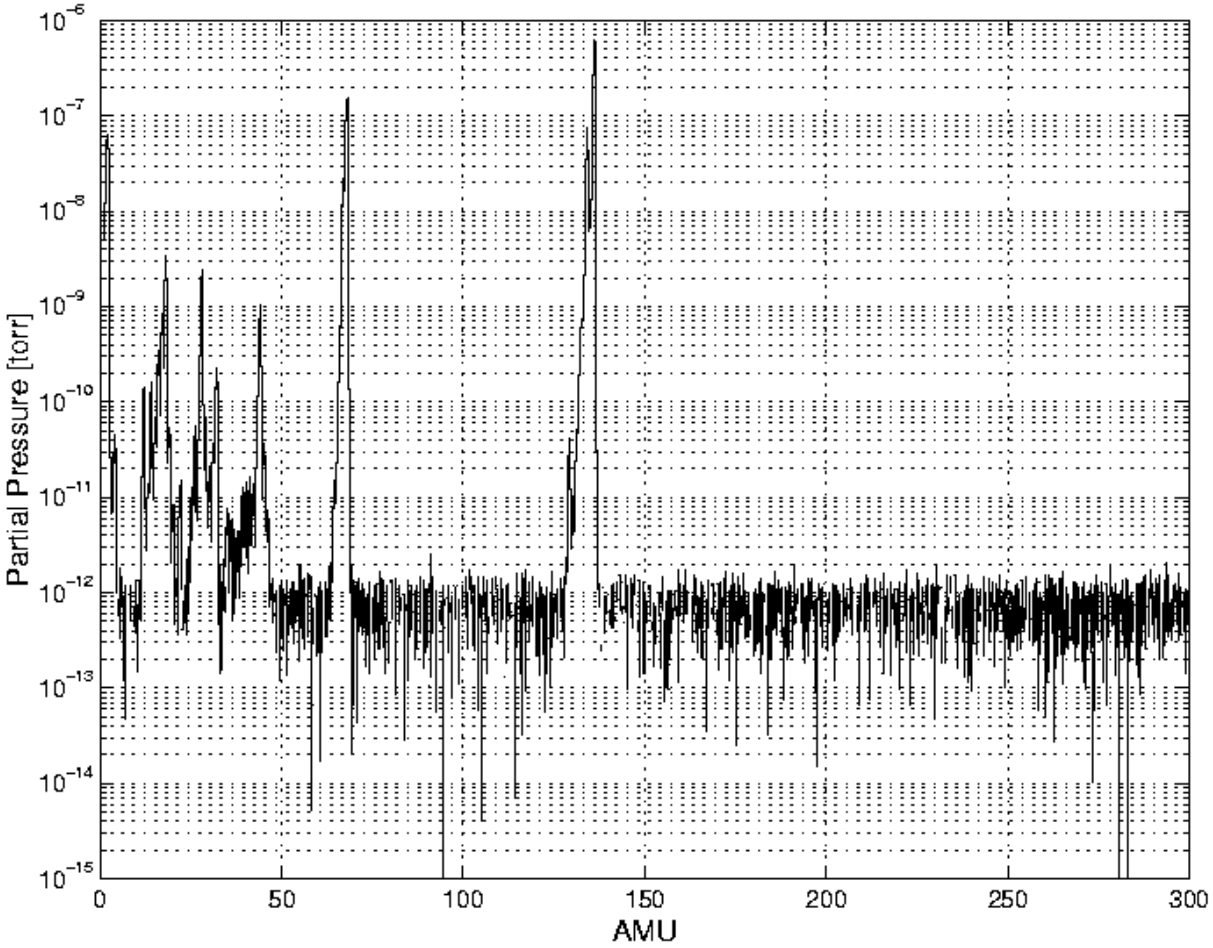

Figure 15: Mass spectrum of the Krasnoyarsk sample of 136-enriched xenon. The peaks around 70 amu are due to doubly ionized xenon. Lower mass peaks are due to vacuum contaminations and are not discussed here.

10^6 of atmospheric Kr is the unstable isotope ^{85}Kr that is radioactive with a $T_{1/2} =$ 10.7 yr. This isotope is produced by nuclear reactors and spent fuel reprocessing plants and it represents a possible background to a double-beta decay experiment. While the similarity of chemical-physical properties of Kr and Xe make it difficult to obtain Kr-free Xe, the isotopic enrichment of the heaviest (136) Xe isotope should automatically provide a very substantial depletion of the much lighter Kr. Indeed, while our measurements of natural Xe show a clear Kr contribution at a level of $(7.7 \pm 1.9) \times 10^{-7}$ Kr/Xe, krypton is not detected in the enriched sample and a limit is set at 6×10^{-7} at 90% CL. While better sensitivities will be reached with a specialized mass spectrometer later this year, this data is already sufficient to assess that the ^{85}Kr contamination should not be a dominant background.

5 100 kg Prototype Detector

A prototype detector to be filled with about 100 kg of ^{136}Xe is an essential component of the R&D work. There are several reasons why such detector is an essential step towards the final multi-tone device:

- A chamber of rather large size is a good test bed for the detector technology to be employed. In particular we believe such chamber should be built to check if the liquid phase is a viable option for the detector. At 100 kg mass the chamber would be close to the largest detector ever built with LXe [48], although special provisions will be made to obtain the best possible resolution with good ionization and scintillation readout.

- Filled with ^{136}Xe such chamber would represent a factor 20 in mass increase respect to the previous largest Xe double-beta decay experiment and will be the largest double beta decay experiment active. In particular the experiment will presumably allow us to measure the $0\nu\beta\beta$ mode that in xenon has eluded detection till now. The knowledge of the $T_{1/2}$ for this mode is an essential element for the design of the final detector, since it represents the irreducible background to be eliminated using the detector's energy resolution.

- A 100 kg LXe detector will also allow us to understand the background situation to be expected in a LXe detector at $2\nu\beta\beta$ decay energies. This will be compared with the data obtained by the Gotthard experiment for a gas-phase detector in the final choice of technology. We note here that the 100 kg prototype will not need the Ba tagging system, rather it will simply serve as a benchmark to evaluate what is the best performance to be expected by the particle detector.

- The production of 100 kg ^{136}Xe will also be an essential part of this phase as it will allow us to develop the logistics of the isotope separation and verify the radiopurity achievable.

The prototype 100 kg chamber will be installed and run either at the new National Underground Science Facility in the Homestake mine or at the DoE Waste Isolation Pilot Plant (WIPP) in New Mexico.

References

[1] K.S. Hirata *et al.* (Kamiokande collab.) Phys. Lett. B205 (1988) 416;
K.S. Hirata *et al.* (Kamiokande collab.) Phys. Lett. B280 (1992) 146;
D. Casper *et al.* (IMB collab.) Phys. Rev. Lett. 66 (1991) 2561;
R. Becker-Szendy *et al.* (IMB collab.) Phys. Rev. Lett. 66 (1991) 2561;
W.W.M. Allison *et al.* (Soudan II collab.) Phys. Lett. B391 (1997) 491;
Y. Fukuda *et al.* (Super-Kamiokande collab.) Phys. Lett. B433 (1998) 9.

[2] C. Athanassopoulos *et al.* (LSND collab.) Phys. Rev. Lett. 81 (1998) 1774;
C. Athanassopoulos *et al.* (LSND collab.) Phys. Rev. C58 (1998) 2489.

[3] B.T. Cleveland *et al.* Astrophys. J. 496 (1998) 505;
M. Cribier *et al.* (Gallex collab.) Nucl. Phys. Proc. Suppl. 70 (1999) 284;
D.N. Abdurashitov *et al.* (SAGE collab.) Nucl. Phys. Proc. Suppl. 70 (1999) 299;
Y. Fukuda *et al.* (Kamiokande collab.) Phys. Rev. Lett. 77 (1996) 1683;
Y. Fukuda *et al.* (Super-Kamiokande collab.) Phys. Rev. Lett. 81 (1998) 1158, Erratum ibid. 81 (1998) 4279.

[4] Y. Fukuda *et al.* (Super-Kamiokande collab.) Phys.Rev.Lett. 81 (1998) 1562.

[5] Q.R. Ahmad *et al.* (SNO collab.) nucl-ex/0106015.

[6] D. O. Caldwell and R. N. Mohapatra, Phys. Rev. D 48 (1993) 3259; J. Ellis and S. Lola, Phys. Lett. B 458 (1999) 310; V. Barger and K. Whisnat, Phys. Lett. B 456 (1999) 194.

[7] S.M. Bilenki *et al.*, Phys. Lett. B465 (1999) 193.

[8] P. Fisher, B. Kayser and K. McFarland, hep-ph/9906244 to appear in Annual Review of Nuclear and Particle Science.

[9] V. Aseev *et al.*, "A Next Generation Tritium Beta Decay Experiment with Sub-eV Sensitivity for the Electron Neutrino Mass", Forschungszentrum Karlsruhe, unpublished.

[10] P. Alivisatos *et al.* (KamLAND design report), Stanford-HEP-98-03, Unpublished;
W. Fulgione, to appear in Proceedings of Neutrino 98, Takayama, Japan, June 98.

[11] L. Wolfenstein, Phys. Rev. D 17 (1978) 2369;
S.P. Mikheyev and A.Yu. Smirnov, Sov. J. Nucl. Phys. 42 (1985) 1441.

[12] M. Apollonio *et al.* Phys. Lett. B420 (1998) 397.

[13] F. Boehm *et al.*, hep-ex/9912050; to appear in Phys. Rev. Lett.

[14] M. Fukugita, G-C. Liu and N. Sugiyama, Phys. Rev. Lett. 84 (2000) 1082.

[15] M. Moe and P. Vogel Ann. Rev. Nucl. Part. Sci. 44 (1994) 247;
M. Moe Int. J. Mod. Phys. E2 (1993) 507;
F. Boehm and P. Vogel in "Physics of massive neutrinos" Chapter 6, Cambridge Univ. Press, 2nd Edition, 1992;
M. Doi, T. Kotani and E. Takasugi Prog. Theor. Phys. 83 (Suppl.) (1985) 1;
W.C. Haxton and G.J. Stephenson Jr. Prog. Part. Nucl. Phys. 12 (1984) 409;
H. Primakoff and S.P. Rosen Rep. Prog. Phys. 22 (1959) 121.

[16] M. Hirsch and H.V. Klapdor-Kleingrothaus Prog. Part. Nucl. Phys. 40 (1998) 323;
M. Hirsch, H.V. Klapdor-Kleingrothaus and S.G. Kovalenko Phys. Lett. B403 (1997) 291;
M. Hirsch, H.V. Klapdor-Kleingrothaus, S. Kolb, S.G. Kovalenko Phys. Rev. D57 (1998) 2020.

[17] F. Boehm and P. Vogel in "Physics of massive neutrinos" Chapter 6, Cambridge Univ. Press, 2nd Edition, 1992.

[18] K. You *et al.* Phys. Lett. B265 (1991) 53.

[19] L. Baudis *et al.* Phys. Lett. B407 (1997) 219; Klapdor, hep-ph/0103062.

[20] S. Elliott *et al.* Phys. Rev. C46 (1992) 1535.

[21] H. Ejiri *et al.* Nucl. Phys. A611 (1996) 85.

[22] A. Sh. Georgadze *et al.*, Phys. Atomic Nucl. 58 (1995) 1093; Danevich, PRC62, 045501 (2000).

[23] A. Alessandrello *et al.* Phys. Lett. B486, 13 (2000). 156.

[24] R. Luescher *et al.* Phys. Lett. B434 (1998) 407;
J.C. Vuilleumier *et al.* Phys. Rev. D48 (1993) 1009.

[25] A. DeSilva *et al.* Phys. Rev. C56 (1997) 2451.

[26] A. Staudt *et al.* Europhys. Lett. 13 (1990) 31;
A. Staudt *et al.* Phys. Lett. B268 (1991) 312.

[27] E. Caurier *et al.* Phys. Rev. Lett. 77 (1996) 1954.

[28] H.T. Wong et al., Phys. Rev. D 48 (1993) 1009. K. Lou et al., Proceedings of the "IV International Symposium on Weak and Electromagnetic Interactions in Nuclei", Edited by H. Ejiri, T. Kishimoto and T. Sato, World Scientific (1995) 192.

[29] C. Brand *et al.* Nucl. Instr. and Meth. A283 (1989) 567.

[30] See for instance "SLS series HV power supplies", Spellman online catalog: http://www.spellmanhv.com.

[31] For a general review on GEMs and other similar devices see: F. Sauli and A. Sharma, CERN-EP/99-69, to appear in Annual Review of Nuclear and Particle Science.

[32] J. Séguinot *et al.*, Nucl. Instr. and Meth. A323 (1992) 583; J. Séguinot *et al.*, Nucl. Instr. and Meth. A354 (1995) 280.

[33] M.K. Moe Phys. Rev. C44 (1991) R931.

[34] M. Danilov *et al.*, Phys. Lett. B480 (2000) 12.

[35] W.B. Atwood *et al.* Nucl. Inst. Meth. A306 (1991) 446.

[36] F. Arneodo *et al.*, hep-ex/9812006, to appear in the proceedings of the "Workshop on New Detectors", Erice, Italy 1997.

[37] H. Dehmelt, Rev. Mod. Physics 62 (1990) 525.

[38] W. Neuhauser, M. Hohenstatt, P. Toschek, and H. Dehmelt, Phys. Rev. Lett. 41 (1978) 233.

[39] E. Ehrlacher and J. Huennekens Phys. Rev. A46 (1992) 2642.

[40] see for example http://

[41] M. Breidenbach *et al.* "EXO proposal for detector R&D" SAGENAP panel, Feb 2000, revised Apr 2000.

[42] J. Engel, P. Vogel, and M. R. Zirnbauer, Phys. Rev. C37 (1988) 731.

[43] M. Guenther *et al.* Phys. Rev. D55 (1997) 54.

[44] D. Dassie *et al.* Phys. Rev. D51 (1995) 2090;
R. Arnold *et al.* Z. Phys. C72 (1996) 239;
A. DeSilva *et al.* Phys. Rev. C56 (1997) 2451.

[45] E. Aprile, R. Mukherjee and M. Suzuki, Nucl. Inst. and Meth. A302 (1991) 177.

[46] A. Bolozdynya *et al.* Nucl. Inst. and Meth. A385 (1997) 225.

[47] J. Seguinot *et al.* Nucl. Inst. and Meth. A323 (1992) 583; J. Seguinot, J Tischhauser and T. Ypsilantis Nucl. Inst. and Meth. A354 (1995) 280.

[48] E. Conti *et al.* Nucl. Inst. and Meth. A356 (1995) 286.

[49] S. Charalambus, Nucl. Phys. A166 (1971) 145.

[50] L. Baudis et al., hep-ex/9811040.

[51] M. Aglietta et al., Il Nuovo Cimento 12C (1989) 467.
M. Aglietta et al., hep-ex/9905047

[52] Y. Giomataris, Nucl. Inst. Meth. A 419 (1998) 239; Y. Giomataris et al. Nucl. Inst. Meth. A 376 (1996) 29

[53] We are thankful to Y. Giomataris for lending us Micromegas foils

[54] C. Amsler *et al.*, Nucl. Inst. and Meth. A 396 (1997) 115

[55] W.S. Gornall and B.P. Stoicheff, Phys. Rev. B4 (1971) 4518.

[56] P. Benetti et.al; Nucl. Instr. and Meth. A 329 (1993) 361

[57] A. Bolotnikov and B. Ramsey, Nucl. Instr. and Meth., A 383 (1996) 619